

The origin of globular cluster systems from cosmological simulations

Kenji Bekki^{1*}, Hideki Yahagi^{2†}, Masahiro Nagashima^{3‡}, and Duncan A. Forbes^{4§}

¹*School of Physics, University of New South Wales, Sydney, NSW 2052, Australia*

²*Division of Theoretical Astronomy, National Astronomical Observatory, 2-21-1 Osawa, Mitaka, Tokyo 181-8588, Japan*

³*Faculty of Education, Nagasaki University, Nagasaki, 852-8521, Japan*

⁴*Centre for Astrophysics & Supercomputing, Swinburne University of Technology, Hawthorn, VIC 3122, Australia*

Accepted, Received 2005 May 13; in original form

ABSTRACT

We investigate the structural, kinematical, and chemical properties of globular cluster systems (GCSs) in galaxies of different Hubble types in a self-consistent manner based on high-resolution cosmological N-body simulations combined with semi-analytic models of galaxy and globular cluster (GC) formation. We focus on correlations between the physical properties of GCSs and those of their host galaxies for $\sim 10^5$ simulated galaxies located at the centres of dark matter halos (i.e. we do not consider satellite galaxies in sub-halos). Our principal results, which can be tested against observations, are as follows. The majority ($\sim 90\%$) of GCs currently in halos are formed in low-mass galaxies at redshifts greater than 3 with mean formation redshifts of $z = 5.7$ (12.7 Gyrs ago) and 4.3 (12.3 Gyrs ago) for metal-poor GCs (MPCs) and metal-rich GCs (MRCs) respectively. About 52 % of galaxies with GCs show clear bimodality in their metallicity distribution functions, though less luminous galaxies with M_B fainter than -17 are much less likely to show bimodality owing to little or no MRCs. The number fraction of MRCs does not depend on Hubble type but is generally smaller for less luminous galaxies. The specific frequencies (S_N) of GCSs are typically higher in ellipticals ($S_N \sim 4.0$) than in spirals ($S_N \sim 1.8$), and higher again ($S_N \sim 5.0$) for galaxies located at the centers of clusters of galaxies. The total number of GCs per unit halo mass does not depend strongly on M_B or Hubble type of the host galaxy. The mean metallicities of MPCs and MRCs depend on M_B such that they are higher in more luminous galaxies, though the dependence is significantly weaker for MPCs. The spatial distributions of MRCs are more compact than those of MPCs and we find that the half-number radii of MPCs ($r_{e,\text{mpc}}$) correlate with the halo masses (M_h) such that $r_{e,\text{mpc}} \propto M_h^{0.18}$. There is no significant difference in velocity dispersions between MPCs and MRCs. We qualitatively compare our results to observational data where possible. Finally, we discuss these results in the wider context of galaxy formation and evolution.

Key words: globular clusters: general – galaxies: star clusters – galaxies: evolution – galaxies: stellar content

1 INTRODUCTION

The physical properties of GCSs in galaxies have long been considered to be “fossil records” that contain vital information on galaxy formation and evolution (e.g., Searle & Zinn 1978; Harris 1991; Ashman & Zepf 1998; West et al.

2004). For example, the observed bimodal colour distributions, higher specific frequencies (S_N) and higher fraction of metal-poor GCs (MPCs) in elliptical galaxies has motivated various formation scenarios for elliptical galaxies (e.g., Ashman & Zepf 1992; Forbes et al. 1997; Côte et al. 1998). Correlations between physical properties of GCSs and those of their host galaxies also have provided clues to the better understanding galaxy formation. For example, Strader et al. (2004) showed that the mean colours of MPCs and MRCs correlate with the luminosity (L) of their host galaxy.

* E-mail: bekki@bat.phys.unsw.edu.au

† E-mail: hideki.yahagi@nao.ac.jp

‡ E-mail: masahiro@nagasaki-u.ac.jp

§ E-mail: dforbes@astro.swin.edu.au

From a survey of Virgo cluster early-type galaxies, Peng et al. (2006, P06) calculated from $g-z$ colours, the relations $[\text{Fe}/\text{H}]_{\text{gc}} \propto L^{0.16 \pm 0.04}$ for MPCs and $[\text{Fe}/\text{H}]_{\text{gc}} \propto L^{0.26 \pm 0.02}$ for MRCs.

In addition to the above chemical property of GCSs, the kinematical and structural properties of GCSs have been investigated both for MPCs and MRCs (Kissler-Patig & Gebhardt 1998; Côte et al. 2001; Rhode & Zepf 2004; Richtler et al. 2004; Peng et al. 2005; Bergond et al. 2006; Bridges et al. 2006; Pierce et al. 2006; Romanowsky 2006; Hwang et al. 2007; Woodley et al. 2007). Peng et al. (2005) showed that the GCS in NGC 5128 has a significant amount of global rotation whereas Richtler et al. (2004) did not find any significant rotation in the GCS of NGC 1399, which suggests a great diversity in the kinematics of GCSs in early-type galaxies. The slopes of power-law density profiles of GCSs are also observed to be diverse and only loosely correlated with the luminosity of their host galaxy (e.g., Harris 1986; Ashman & Zepf 1998).

In comparison with this remarkable progress in observational studies of GCSs (Brodie & Strader 2006), theoretical modeling has not been as well developed as to provide useful predictions that can be compared with the wide range of observations on GCS properties. This is mainly because, both *subpc-scale* formation processes of GCs in galaxies and *kpc- and Mpc-scales* merging/interaction processes over a Hubble time need to be modeled in a fully self-consistent manner in order that the GCS properties and GCS-host relations can be examined quantitatively.

Beasley et al. (2002; B02) first investigated the physical properties of GCSs and their correlations with those of host galaxies based on a semi-analytic model of hierarchical galaxy formation in a Λ CDM universe. B02 however could not discuss the structural and kinematical properties of GCSs owing to the limitations of the adopted semi-analytic model. Although previous collisionless N-body simulations with GCs have provided some reasonable explanations for the origin of structural and kinematical properties of GCSs (e.g., Bekki et al. 2005; Bekki & Forbes 2006), they did not model the chemical properties of GCSs. Kravtsov & Gnedin (2005) carried out a high resolution gas + N-body simulation of GC formation in a Λ CDM universe. In their model of a Milky Way like galaxy, GCs first formed at redshift ~ 12 with peak formation occurring at $z \sim 4$. However they only simulated MPCs and only from formation to a redshift of 3. Thus no simulations have yet addressed the structural, kinematical, and chemical properties of GCSs in a self-consistent cosmologically motivated simulation from formation to the current epoch.

The purpose of this paper is to investigate *both the dynamical and chemical properties* of GCSs based on cosmological N-body simulations with semi-analytic models of galaxy formation and thereby compare the results with the above-mentioned growing number of observational constraints on GCS-host relations. We focus particularly on the following physical properties of GCSs in galaxies : (i) GC metallicity distribution functions (MDFs), (ii) number fractions of MRCs (f_{mrc}), (iii) number fractions of GCS with bimodal MDFs (f_{bimo}), (iv) specific frequencies of GCs (S_{N}), (v) mean GCS metallicities ($[\text{Fe}/\text{H}]$), (vi) GCS half-number radii (r_e), and (vii) GCS velocity dispersions (σ). We mainly investigate correlations between these GCS properties and

their host properties such as M_{B} and Hubble type. Here we do not discuss other important observational results of GCSs, such as the blue tilt (e.g., Strader et al. 2006) or the GC luminosity function dependence on galaxy luminosities (e.g., Jordán et al. 2006). Some of these aspects have been already discussed in our previous papers (e.g., Bekki et al. 2007a, B07). Here we also restrict our analysis to central galaxies and do not consider satellites in sub-halos.

The plan of this paper is as follows: In the next section we describe our numerical method of cosmological N-body simulations, semi-analytic model of galaxy formation, and formation model for GCs. In §3, we present our numerical results on GCS properties in galaxies with different luminosities and Hubble types. In §4, we discuss our results of GCS-host relations in the context of galaxy formation and evolution. We summarize our conclusions in §5.

2 THE MODEL

We consider that GCs can be formed within any galaxy at any redshift, if the physical conditions required for GC formation are satisfied in the galaxies. We therefore investigate GC formation rates in any virialized halo in a high-resolution cosmological simulation based on a Λ CDM cosmology model. The physical properties of GCs (e.g., metallicities) are determined by their host galaxies at the epoch of their formation. GCs formed in low-mass galaxies at high z can be tidally stripped during the hierarchical merging of galaxies to finally become GCs within a giant galaxy at $z = 0$. Since numerical methods and techniques of the present cosmological simulations and those of semi-analytic models of galaxy formation have been given in our previous papers (e.g., Yahagi et al. 2004; Nagashima et al. 2005, N05), we only briefly describe them in the present study. We here focus on (i) how to identify GCs in virialized dark matter halos and (ii) how to allocate physical properties to the identified GCs based on their host galaxy properties.

2.1 Simulations

We simulate the large scale structure of GCs in a Λ CDM Universe with $\Omega = 0.3$, $\Lambda = 0.7$, $H_0 = 70 \text{ km s}^{-1} \text{ Mpc}^{-1}$, and $\sigma_8 = 0.9$ by using the Adaptive Mesh Refinement N-body code developed by Yahagi (2005) and Yahagi et al. (2004), which is a vectorized and parallelized version of the code described in Yahagi & Yoshii (2001). We use 512^3 collisionless dark matter (DM) particles in a simulation with the box size (R_{T}) of $70h^{-1} \text{ Mpc}$ and the total mass (M_{T}) of $4.08 \times 10^{16} M_{\odot}$. We start simulations at $z_i = 41$ and follow it until $z = 0$ in order to investigate the physical properties of GCs outside and inside of virialized dark matter halos. We use COSMICS (Cosmological Initial Conditions and Microwave Anisotropy Codes), which is a package of Fortran programs for generating Gaussian random initial conditions for non-linear structure formation simulations (Bertschinger 1995, 2001).

Our method of identifying GCs (or ‘‘GC particles’’) and following their evolution is described as follows. Firstly, we select virialized dark matter subhalos at a given redshift by using the friends-of-friends (FoF) algorithm (Davis et al. 1985) with a fixed linking length of 0.2 times the mean DM

Table 1. Model parameters in the simulation.

Ω	Λ	H_0 (km s ⁻¹ Mpc ⁻¹)	σ_8	M_T ^a	R_T ^b	z_i ^c	z_{trun} ^d	α ^e	β ^f	SNe feedback ^g
0.3	0.7	70	0.9	4.08	70	41	6	0.02	0.05	strong

^a The total mass of a simulation in units of $10^{14} M_\odot$.

^b The box size of a simulation in units of h^{-1} Mpc

^c The redshift (z) at which a simulation starts.

^d The redshift of truncation of GC formation: GC formation is completely truncated in halos that are virialized later than the redshift.

^e The coefficient in the functional form describing the dependence of GC formation rate on the mass ratios of merging two galaxies.

^f The coefficient in the functional form describing the dependence of GC formation rate on the gas mass fractions of galaxies.

^g The details of the strong and weak feedback effects are given in N05.

particle separation. The minimum particle number N_{min} for halos is set to be 10. For each individual virialized subhalo, the central particle is labeled as a ‘‘GC’’ particle. This procedure for defining GC particles is based on the assumption that energy dissipation via radiative cooling allows baryons to fall into the deepest potential well of dark matter halos and finally to be converted into GCs and stars.

The adopted initial distributions of GCs with respect to their host halos would be oversimplified, given that possible candidates of forming GCs are not necessarily in the central regions of galaxies at $z = 0$. We think that the adopted assumption can be regarded as reasonable, because previous observations suggested that a significant fraction (or even all) of the Galactic GCs originate from nuclei of the Galactic building blocks at high z (e.g., Zinnecker et al. 1988; Freeman 1993). We stress that the predicted spatial distributions of GCSs in galaxies at $z = 0$ might well weakly depend on the adopted initial distributions of GCs within halos, though previous simulations suggested that distributions of GCSs at $z = 0$ do not depend strongly on the adopted range of reasonable initial GC distributions (Yahagi & Bekki 2005).

Secondly, we follow GC particles until $z = 0$ and thereby derive their locations (x, y, z) and velocities (v_x, v_y, v_z). We then identify virialized halos at $z = 0$ with the FoF algorithm and investigate whether each GC is within the virial radius (r_{vir}) of a halo. If GCs are found to be within a halo, the physical properties of the GCS are investigated. If a GC is not in any halo, it is regarded as an intergalactic GC. We don’t discuss these intergalactic (i.e., intra-group and intra-cluster) GCs further in this current paper (see Yahagi & Bekki 2005; Bekki & Yahagi 2006 for details of such GCs), though a growing number of observations have revealed physical properties of these intergalactic GCs (e.g., Bassino et al. 2006; Jones et al. 2006).

Recent theoretical works have suggested that heating and gas loss resulting from reionization can severely suppress star formation in low-mass galaxies during reionization (e.g., Susa & Umemura 2004). It is therefore highly likely that GC formation is truncated in low-mass galaxies that are virialized after the completion of reionization. In order to include the effects of the suppression of GC formation via reionization on the final properties of the simulated GCSs, we adopt the following somewhat idealized assumption: If a galaxy is virialized after the completion of reionization (z_{reion}), then GC formation is totally suppressed in the galaxy. Therefore, GC particles formed in galaxies with $z_{\text{vir}} < z_{\text{reion}}$ are not considered in the physical properties of the simulated GCSs. We define the truncation epoch of GC

formation as z_{trun} (rather than z_{reion} for convenience) in the present study. Recent quasar absorption-line studies give a lower limit of 6.4 for z_{reion} (Fan et al. 2003). Guided by these observations, we investigate the model with $z_{\text{trun}} = 6$.

Thus the GCS of a galaxy is a collection of GCs that are formed within low-mass galaxies (i.e., galaxy building blocks) embedded in massive dark matter halos virialized at high redshifts. The physical properties of the GCS of a galaxy therefore depends on star formation histories, chemical evolution, and merging histories of the building blocks. Chemical evolution and star formation histories of building blocks for galaxies are derived from the semi-analytic model (N05) which are based on the merging histories of DM halos derived from our N-body simulation.

2.2 Semi-analytic model

The physical properties of a newly formed GC in a virialized halo at any redshift are determined by those of its host galaxy at that redshift. N05 constructed the Numerical Galaxy Catalog (ν GC) based on a semi-analytic model combined with high-resolution N -body simulations. In the present study, we adopt the same semi-analytic model as that used by N05 which includes various physical processes associated with galaxy formation, such as galaxy merging, radiative gas cooling, star formation, supernovae feedback, and extinction by internal dust. Since the methods and techniques are given in detail by N05, we do not describe them in the present study.

The semi-analytic model by N05 can reproduce many observations reasonably well, such as cold gas mass-to-stellar luminosity ratios of spiral galaxies, faint galaxy number counts, cosmic star formation rates, the Tully-Fisher relation for bright spiral galaxies, luminosity functions of local galaxies, and colour-magnitude relations for massive and dwarf elliptical galaxies. The successes and limitations of this model in explaining observed galactic properties are given in N05.

Here we present the results for the properties of GCs from our semi-analytic model and compare them where possible to observations. We focus on results from the model with the ‘‘strong feedback effects’’ (N05) in which galaxies with smaller rotational velocities are much more strongly influenced by heating. An important caveat in this work is that only galaxies located at the centers of halos are analyzed in the present study, i.e. we do not investigate satellite galaxies. Thus we effectively focus on brightest cluster, brightest group and isolated galaxies in this current work. Observational studies are often dominated by non-central galaxies

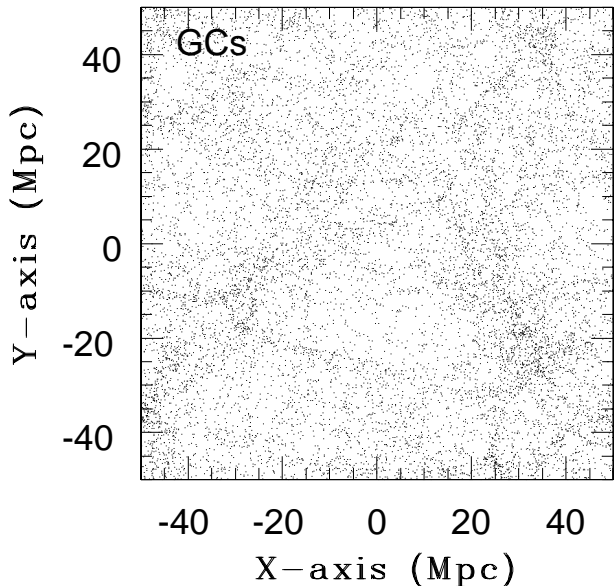


Figure 1. The distribution of GCs projected onto the x - y plane at $z = 0$. Here only GC particles that are at the very centers of GCSs for galaxies at $z = 0$ are shown for convenience. Thus the distribution describes the large-scale distribution of GCSs of galaxies in the universe at $z = 0$.

(satellites in this context) and this should be born in mind when we compare our model predictions to the observations below.

2.3 Formation efficiencies of GCs

We convert the star formation rate (SFR) in a galaxy into a GC formation rate (GCFR) based on the physical properties of the host galaxy at a given redshift. The vast majority of stars are observed to form in star clusters (SCs) embedded within GMCs (Lada & Lada 2003). Strongly bound SCs can evolve into GCs or old open clusters whereas weakly bound, low-mass ones can be disintegrated into field stars of the host galaxy. The mass fraction of new SCs that evolve into GCs relative to all new SCs is denoted as C_{eff} and is assumed to be dependent on the physical properties of their host galaxy. Thus we define the GCFR as:

$$\text{GCFR} = C_{\text{eff}} \times \text{SFR}, \quad (1)$$

where SFR is an output from the semi-analytic model.

We consider both observational results by Larsen & Richtler (2000, LR00) and simulation ones by Bekki et al. (2002, BFBC02) in order to determine C_{eff} in a physically reasonable way. LR00 investigated correlations between specific U -band cluster luminosities $T_L(U)$ of GCSs and their host galaxy properties both for apparently isolated galaxies and for interacting/merging ones. LR00 found that (i) $T_L(U)$ correlates with SFR per unit area, stellar surface brightness, and HI surface density, and (ii) $T_L(U)$ is more than an order of magnitude higher in strongly starbursting mergers (e.g., NGC 1705) than apparently normal galaxies that are forming young SCs (see Table 1 in LR00). These results by LR00 imply that C_{eff} can be higher in galaxies with higher surface densities and higher gas mass fractions for a given galaxy luminosity.

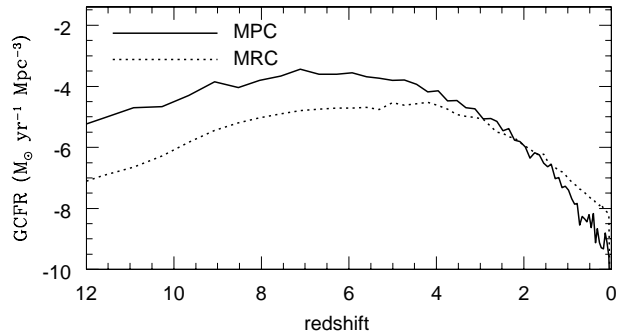


Figure 2. Cosmic evolution of GC formation rates (GCFRs) as a function of redshift (z) for MPCs (solid) and MRCs (dotted). The GCFRs are averaged over the volume of the simulation.

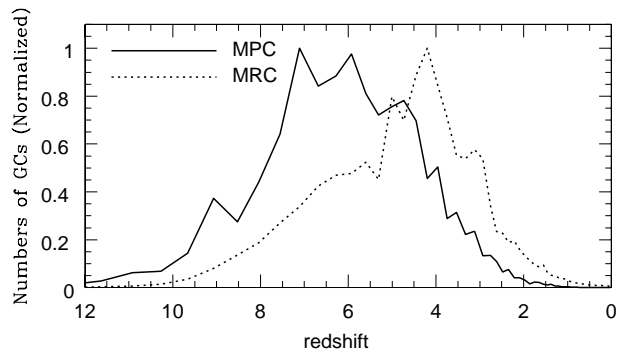


Figure 3. Total numbers of GCs formed at redshift z for MPCs (solid) and MRCs (dotted). The numbers are normalized by the maximum values for $0 \leq z \leq 12$.

Numerical simulations of GC formation in merging galaxies (BFBC02) found that C_{eff} depends on the mass ratios of the merging spirals (f_m or m_2) and their gas mass fractions (f_g) in such a way that C_{eff} is higher in mergers with larger m_2 and f_g . These results by BFBC02 combined with LR00 imply that C_{eff} is a minimum for isolated galaxies with $m_2 = 0$ and maximum for equal mass galaxy mergers with $m_2 = 1$. BFBC02 also found that C_{eff} is lower in low surface brightness galaxies for a given galaxy mass. Galaxies with their halos virialized at higher z have more compact disks and thus higher stellar densities for a given mass, baryonic mass fraction, spin parameter, and halo circular velocity in galaxy formation models based on Λ CDM (e.g., Mo et al. 1998). The above result by BFBC02 combined with that by Mo et al. (1998) therefore strongly suggests that C_{eff} is likely to be higher for galaxies formed at higher z . Thus C_{eff} is a function of the gas fraction, the merger mass ratio and formation redshift.

We estimate C_{eff} as follows:

$$C_{\text{eff}} = C_0 F_g(f_g) F_m(f_m) F_z(z). \quad (2)$$

We need to choose the forms of these three functions (F_g , F_m , and F_z) so that they are consistent with previous results by LR00 and BFBC02. The normalization factor C_0 is determined as follows:

$$C_0 = F_{g,\text{max}}^{-1} F_{m,\text{max}}^{-1} F_{z,\text{max}}^{-1}, \quad (3)$$

where $F_{g,\text{max}}$, $F_{m,\text{max}}$, and $F_{z,\text{max}}$ are maximum values of the above three functions. This method of normalization ensures

that C_{eff} is always equal to or less than 1. If we adopt a value of C_0 significantly smaller than the one given in the above equation, physical properties of the simulated GCSs (e.g., total numbers of GCs in galaxies) can be much less consistent with observations.

In the present study, we choose elementary functions for C_{eff} . Considering that (i) the dependence of C_{eff} on f_m appears to be non-linear (BFBC02) and (ii) C_{eff} is much higher in major mergers (LR02 and BFBC02), we assume the following:

$$F_m(f_m) = 1 - (1 + \alpha)^{-1} + (1 + \alpha - f_m)^{-1}, \quad (4)$$

where α is a parameter. This formula ensures that $F_m(f_m)$ has a minimum (= 1) at $f_m = 0$ corresponding to isolated disk galaxies and a maximum at $f_m = 1$ corresponding to major mergers. Furthermore, if a small value of α (< 0.1) is adopted, F_m is more than 10, which corresponds to a strongly starbursting major merger in LR00. We adopt the same functional form for $F_g(f_g)$:

$$F_g(f_g) = 1 - (1 + \beta)^{-1} + (1 + \beta - f_g)^{-1}. \quad (5)$$

Thus, α and β are free parameters which are chosen so that observations of GCSs can be self-consistently explained.

Mo et al. (1998) showed that the sizes (R_d) of disk galaxies formed at redshift z are inversely proportional to $H(z)/H_0$ for given disk and halo properties (e.g., disk mass fraction and halo circular velocity). Therefore R_d can be more compact for disk galaxies formed at higher redshifts so that mean stellar densities Σ_s within R_d ($\Sigma_s \propto R_d^{-2}$ for a given stellar disk mass) are higher. Considering the above dependences of disk properties on $H(z)/H_0$ (Mo et al. 1998), we adopt the following functional form:

$$F_z(z) = (H(z)/H_0)^2. \quad (6)$$

We estimate $F_z(z)$ for each halo at a given redshift based on the virialization redshift (z_{vir}) of the halo.

Here we adopt a simpler yet qualitatively reasonable dependence of $F_z(z)$: we do not directly derive the surface mass densities by assuming initial sizes of halos, spin parameters, and sizes of galaxies based on the results of the SAM by N05. Although we can not discuss the importance of these physical properties (e.g., initial spin parameters) in GC formation in the present model, we can show the importance of surface mass (or gas) densities (i.e., the epoch of virialization) in GC formation of galaxies in a clearer and more straightforward way thanks to the adopted model. It should be stressed here that without introduction of the $F_z(z)$, most GCS properties can not be reproduced well in the present model.

Although the adopted functional forms of F_m , F_g , and F_z are reasonable at least qualitatively, no observations have been carried out which allow us to determine whether the adopted functional form is quantitatively consistent with observations. Accordingly other functional forms could be adopted so that observational properties of GCSs can be reproduced as well. Here we do not discuss the results of models with different functional forms of F_m , F_g , and F_z .

$T_L(U)$ in some merging galaxies (e.g., NGC 1705) are observed to be as large as 15, which is a factor of ~ 20 larger than the average value (= 0.7) of $T_L(U)$ for non-merging galaxies with young GCs (LR00). Also there is a factor of ~ 200 difference between the minimum (=0.07) and

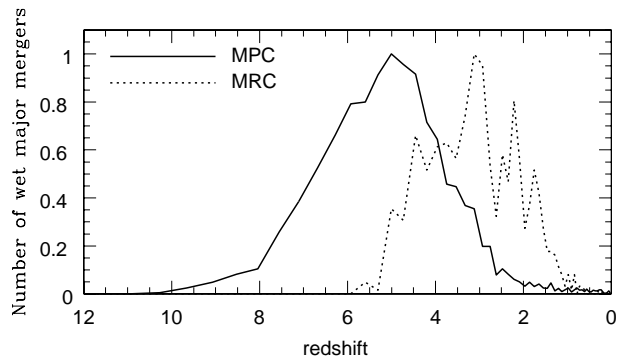


Figure 4. Number of gas-rich (“wet”) major mergers that form MPCs (solid) and MRCs (dotted) as a function of z . Here wet major mergers are those with $f_g > 0.5$ and $f_m > 0.5$. The numbers normalized by their maximum values for $0 \leq z \leq 12$ are shown.

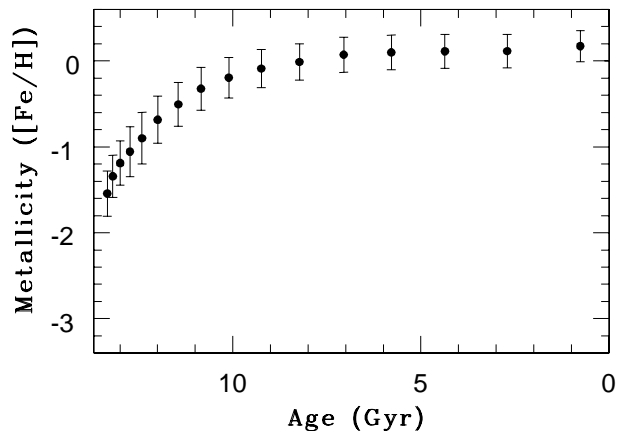


Figure 5. The age-metallicity relation for all GCs. The mean metallicity of GCs in age bins are shown by filled circles. The 1σ dispersion in the metallicities of GCs for each age bin is shown by an error bar.

maximum (=15) values of $T_L(U)$ for galaxies with young GC candidates in LR00. Therefore $0.005 \leq \alpha \leq 0.05$ is a reasonable range of α in F_m . We try to determine the most reasonable values of α and β for which both the observed net formation efficiency of GCs (McLaughlin 1999) and the number fraction of MRCs (Spitler et al. 2007) can be well reproduced by the present simulation.

The net formation efficiency of GCs (ϵ) in the present study is defined as follows:

$$\epsilon = \frac{M_{\text{gc}}}{M_{\text{star}}}, \quad (7)$$

where M_{gc} and M_{star} are total masses of GCs and stars, respectively, which are formed in *all* building blocks in the simulation. We define f_{mrc} as follows:

$$f_{\text{mrc}} = \frac{N_{\text{mrc}}}{N_{\text{mpc}} + N_{\text{mrc}}}, \quad (8)$$

where N_{mpc} and N_{mrc} are numbers of MPCs and MRCs, respectively. Since we find that the model with $\alpha = 0.02$ and $\beta = 0.05$ can best reproduce the observations, we discuss this model in this paper.

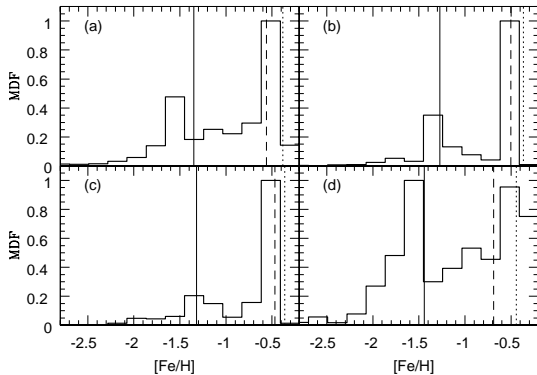


Figure 6. Metallicity distribution functions (MDFs) for four representative massive galaxies with $\log_{10}(\frac{M_h}{M_\odot}) \geq 13.0$: (a) $M_B = -20.7$ mag and $B/T = 1.0$, (b) $M_B = -21.3$ mag and $B/T = 1.0$, (c) $M_B = -21.3$ mag and $B/T = 1.0$, and (d) $M_B = -20.9$ mag and $B/T = 1.0$. The mean metallicities of MPCs, MRCs, and all GCs are shown by solid, dotted, and dashed lines, respectively. Although the shapes of MDFs are different in different galaxies, they all clearly show bimodal MDFs.

2.4 Main points of analysis

The total number of virialized halos at $z = 0$ is 95139, among which only 12179 (thus 12.8 %) have GCs that are formed in their building blocks virialized before $z = 6$ (i.e., reionization). The total number of *GC particles* at $z = 0$ is 998529 in the present simulation. Fig. 1 shows the large-scale structure of GCs that are in the very central regions of their host galaxies at $z = 0$. Although these central GCs in galaxies are relatively metal-rich with a mean metallicity of $[\text{Fe}/\text{H}] = -0.18$ for the 12179 galaxies, some fraction of them (37.5%) are metal-poor ($[\text{Fe}/\text{H}] < -1$). Here we focus on correlations between physical properties of GCSs and those of their host galaxies: we do not discuss the internal properties of individual GCSs.

In investigating GCS properties, we divide GCs into MPCs and MRCs according to their metallicities ($[\text{Fe}/\text{H}]$): those with $[\text{Fe}/\text{H}] < -1$ and with $[\text{Fe}/\text{H}] \geq -1$ are defined as MPCs and MRCs, respectively. We investigate the physical properties of GCSs separately for these two GC subpopulations. We also discuss the bimodality in the metallicity distribution functions (MDFs) of GCSs. We show some examples of individual representative GCSs in Appendix A.

Following the morphological classification scheme by Simien & de Vaucouleurs (1986), we classify simulated galaxies into three different morphological types: E, S0, and Sp. We use the simulated B-band bulge-to-disk luminosity ratio, B/D in the above morphological classification. In this paper, galaxies with $B/D > 1.52$, $0.68 < B/D < 1.52$, and $B/D < 0.68$ are classified as elliptical (E), lenticular (S0), and spiral galaxies (Sp), respectively.

3 RESULTS

3.1 Cosmic evolution

Since our main focus is to discuss the results of correlations between physical properties of GCSs and those of their host galaxies at $z = 0$, we do not discuss the cosmic evolution of

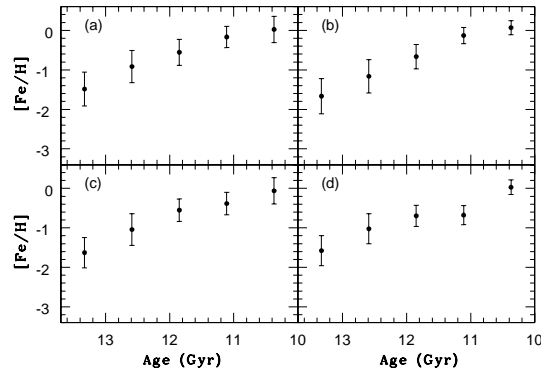


Figure 7. The age-metallicity relations (AMRs) of GCs for the four galaxies shown in Fig. 6. The mean metallicities of GCs are shown for the five age bins. In order to show the AMRs more clearly, only GCs with ages larger than 10 Gyr as few younger GCs are present. The 1σ dispersion in the metallicities of GCs for each age bin is shown by an error bar.

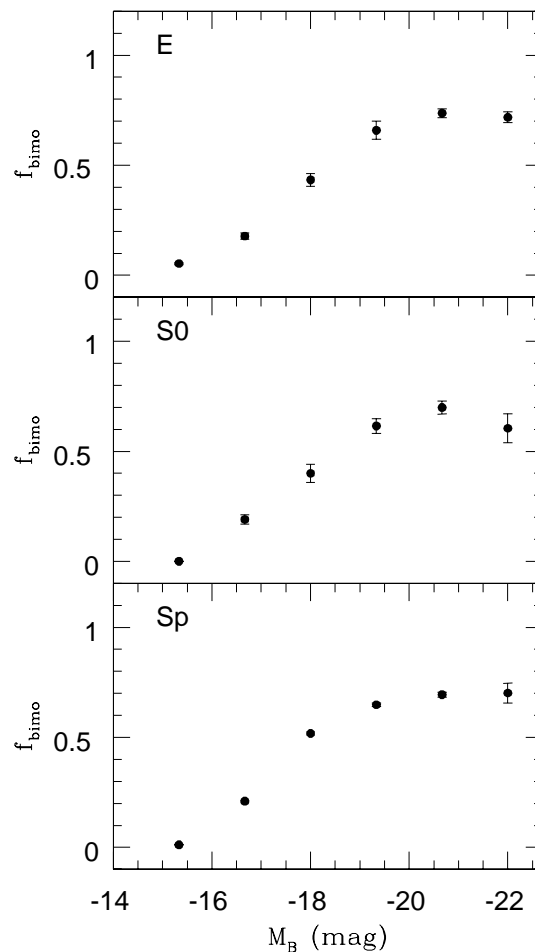


Figure 8. The number fractions of GCSs with bimodal MDFs (f_{bimo}) as a function of M_B for Es (top), S0s (middle), and Sp (bottom). The error bar in each bin is based on Poisson \sqrt{N} statistics.

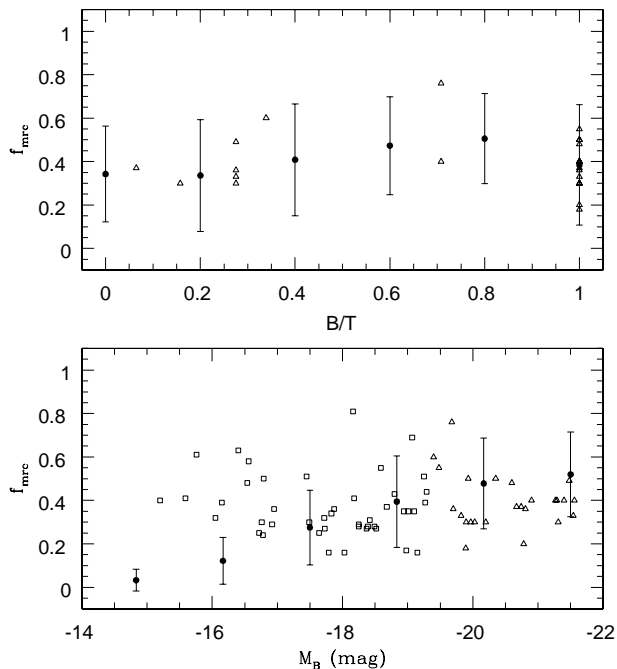


Figure 9. Distributions of the simulated GCSs in the $f_{\text{mrc}}-B/T$ plane (upper) and the $f_{\text{mrc}}-M_B$ one (lower), where f_{mrc} is the number fraction of MRCs in a GCS. Triangles and squares represent the observational results by Spitler et al. (2007) and by P06, respectively, whereas circles show the average values of f_{mrc} in B/T and M_B bins. The 1σ dispersion for each bin is shown by an error bar.

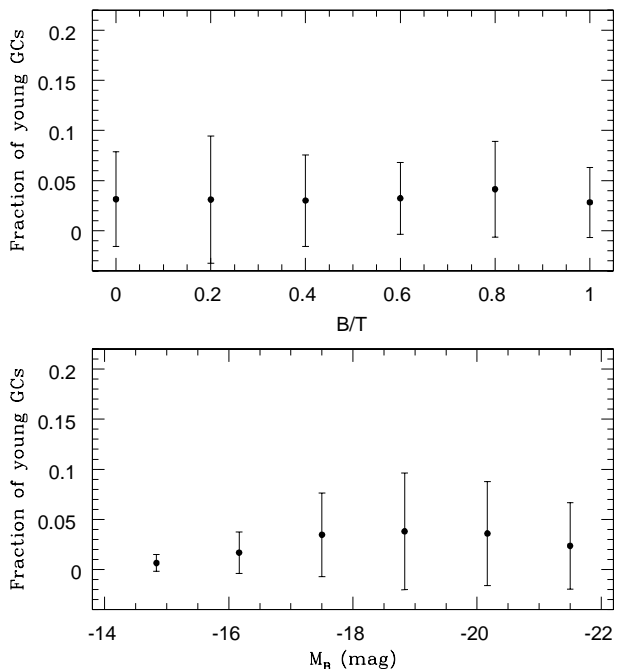


Figure 10. Distributions of the simulated GCSs on the f_y-B/T plane (upper) and on the f_y-M_B one (lower), where f_y is the number fraction of young MRCs with ages less than 8 Gyrs. Circles show the average values of f_y in B/T and M_B bins. The 1σ dispersion for each bin is shown by an error bar.

Table 2. Metallicity-luminosity relations. The observed (o; Peng et al. 2006) and simulated (s) coefficients are given for MPC, MRC and all GCs, where $[\text{Fe}/\text{H}] = a + b M_B$.

	a_o	b_o	a_s	b_s
MPC	-2.771	-0.064	-2.414	-0.052
MRC	-2.452	-0.105	-2.056	-0.081
All	-4.854	-0.206	-3.910	-0.160

GCS. We do however briefly summarize the cosmic evolution of GCS properties *averaged over all GCs formed in the simulation*. Fig. 2 shows that the peaks of cosmic GCFRs are at $z \sim 7$ for MPCs and at $z \sim 4$ for MRCs and that the GCFR is much higher in MPCs than in MRCs at $z > 2$, whereas it is higher in MRCs for $z < 2$. Fig. 3 shows that number distributions of MPCs and MRCs normalized by their maximum values have two different peaks, which reflect the differences in cosmic evolution of GCFRs between MPCs and MRCs.

Fig. 4 shows that both MPCs and MRCs can be formed from gas-rich ($f_g > 0.5$), major ($f_m > 0.5$) mergers for a wide range of redshifts and that formation rates of MPCs and MRCs from wet major mergers peak at $z \sim 5$ for MPCs and at $z \sim 3$ for MRCs. As shown in Fig. 5, the mean metallicities for all GCs (including both MPCs and MRCs) steeply increase for ages > 10 Gyr as a result of rapid chemical enrichment in the building blocks of galaxies. The time evolution of the mean metallicities appears to be much less dramatic for ages < 10 Gyr owing to the slower chemical enrichment processes in galaxies. The dispersions in the mean metallicities ($\sigma(\text{Fe}/\text{H})$) are smaller for larger ages i.e., older GCs. We find $\sigma(\text{Fe}/\text{H}) \sim 1.6$ dex for ~ 13 Gyr and $\sigma(\text{Fe}/\text{H}) \sim 0.1$ dex for ~ 0.8 Gyr.

It is interesting to derive the age-metallicity relation of GCs with ages t (Gyr) older than 10 Gyr in the present simulation at $z = 0$ in order to compare the simulated relation with the observed one when sufficient observational results are available. The χ -square fit to the simulation data gives the following:

$$[\text{Fe}/\text{H}] = 10.86 - 10.83 \log_{10} t \quad (9)$$

The model predicts the presence of young (< 3 Gyr) GCs with $[\text{Fe}/\text{H}] > 0$, though the number fraction of such GCs is quite small. Most of these metal-rich GCs are found to be located in the central regions of galaxies in the simulation. It should be however stressed that very old (> 13 Gyr), metal-poor ($[\text{Fe}/\text{H}] < -1.6$) GCs can also be found in the very central regions of galaxies at $z = 0$.

3.2 Metallicities and ages

Fig. 6 shows that the GCSs in four early-type galaxies with $B/T \approx 1$ at $z = 0$ have bimodal MDFs with peaks below and above $[\text{Fe}/\text{H}] = -1$. The locations of the two peaks and the number ratios of GCs in each peak are different between different galaxies, which implies that merging and star formation histories of their building blocks are quite diverse in the four galaxies. The peak metallicities of GCSs reflect the gaseous metallicities of the building blocks at the epoch when strong starbursts were triggered mostly by gas-rich (“wet”), major merging at high z (> 3). Although these four galaxies located in the centers of massive clusters of galaxies with $M_h > 10^{13} M_\odot$ clearly show bimodal MDFs,

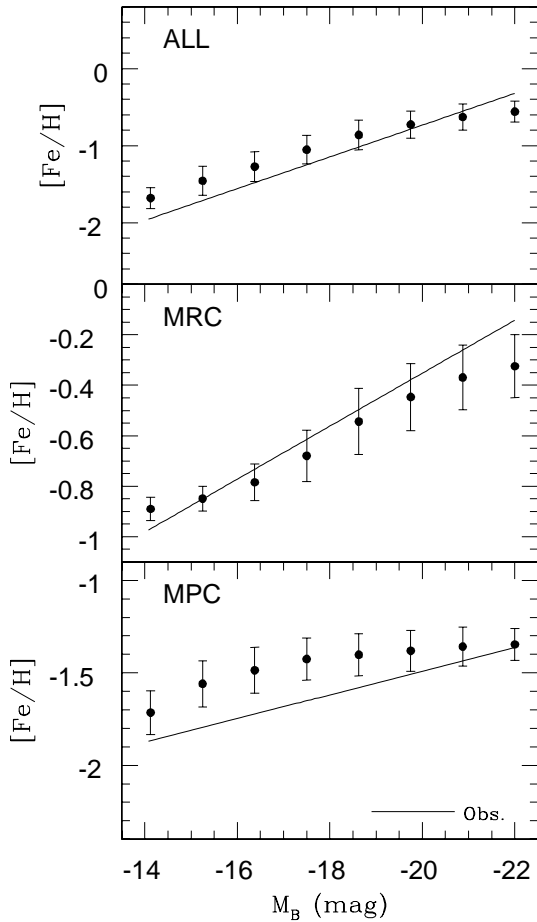


Figure 11. Distributions of the simulated GCSs in the M_B - $[\text{Fe}/\text{H}]$ plane for all GCs (top), MRCs (middle), and MPCs (bottom). Here $[\text{Fe}/\text{H}]$ represents the mean metallicity of a GCS in a galaxy. Circles show the average values of $[\text{Fe}/\text{H}]$ in a M_B bin. The 1σ dispersion for each bin is shown by an error bar. For comparison, the observed M_B - $[\text{Fe}/\text{H}]$ relations of P06 are shown by solid lines in the three panels.

less luminous galaxies in the field and groups of galaxies do not necessarily show bimodal MDFs in their GCSs. The diverse shapes of MDFs of these galaxies (including those that show unimodal MDFs) are briefly discussed in Appendix A.

Fig. 7 clearly shows that younger GCs are likely to be more metal-rich for all four galaxies and that the age-metallicity relations are similar to one another. Since the colours of GCs depend on both age and metallicity, these results suggest that the colour distributions of the simulated GCSs will be somewhat different from their MDFs. On the other hand, the GCSs are dominated by very old GCs in each case. We plan to investigate whether the colour distributions of GCSs are consistent with observations by combining the present GC formation model with a stellar population synthesis code and the effects of photometric uncertainty in a future paper.

To investigate the number fractions (f_{bimo}) of galaxies that reveal clear bimodal MDFs we determine f_{bimo} as follows:

$$f_{\text{bimo}} = \frac{N_{\text{bimo}}}{N_{\text{gal}}}, \quad (10)$$

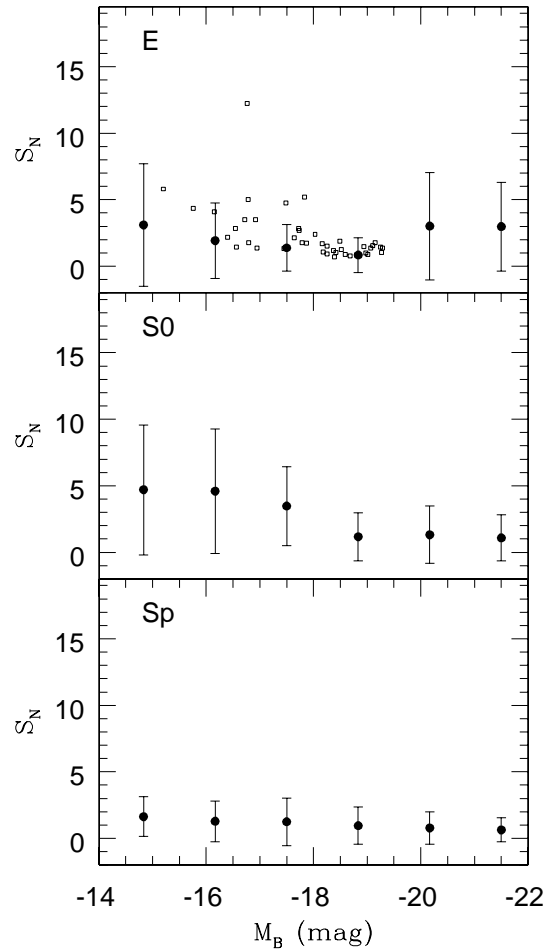


Figure 12. Distributions of the simulated GCSs in the S_N - M_B plane for E (top), S0 (middle), and Sp (bottom). Circles show the average values of S_N in a M_B bin. Open squares represent the observational results by P06, for which we assume that $B - V = 0.9$ for all Es to estimate S_N . The 1σ dispersion for each bin is shown by an error bar.

where N_{bimo} and N_{gal} are the number of galaxies with obviously bimodal GCS MDFs and that of all galaxies, respectively. In the present study, an MDF with obvious bimodality is defined as revealing a clear metallicity peak at both low ($[\text{Fe}/\text{H}] < -1$ for MPCs) and high metallicity ($[\text{Fe}/\text{H}] \geq -1$ for MRCs).

Fig. 8 shows that more than 70% of galaxies with $M_B < -19$ mag have bimodal MDFs in their GCSs regardless of their Hubble types. The number fraction of GCSs with bimodal MDFs (f_{bimo}) depends on M_B such that less luminous galaxies have smaller f_{bimo} (i.e., less likely to have bimodal MDFs). Considering that we do not include GCSs with no MPCs in estimating f_{bimo} , the above result means that only MPCs are formed in the building blocks of these less luminous galaxies with no bimodal MDFs. Furthermore gas-rich, major merging between high-density building blocks does not occur after their gaseous metallicities becomes higher than $[\text{Fe}/\text{H}] \sim -1$ in the formation histories of these galaxies.

Fig. 9 shows that the number fraction of MRCs (f_{mrc}) does not depend on B/T . Some very late-type spirals with $B/T < 0.05$ have high values of f_{mrc} (> 0.6) whereas some

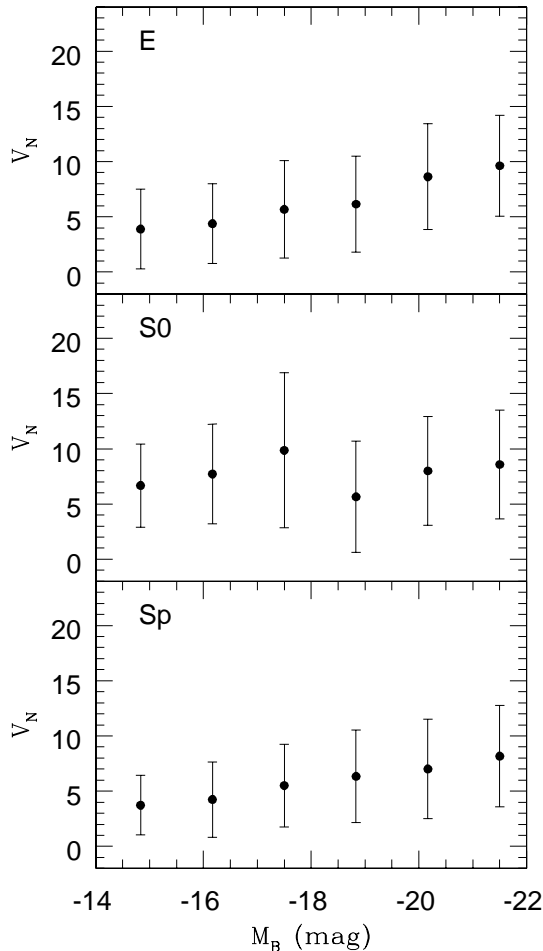


Figure 13. The same as Fig. 12 but for the V_N - M_B plane, where V_N is the number of GCs per halo mass.

ellipticals with $B/T \approx 1$ have low values of $f_{\text{mrc}} (< 0.1)$, which suggests that the origin of the Hubble types of galaxies are not closely associated with the metal-rich fraction (f_{mrc}) in their GCSs. However f_{mrc} does depend on M_B such that f_{mrc} is higher in more luminous galaxies, though the dispersions in f_{mrc} are quite large over a wide range of M_B . Galaxies with $M_B < -20$ mag cover a similar range for observed galaxies in the $M_B - f_{\text{mrc}}$ plane (Spitler et al. 2007). The mean value of f_{mrc} for all GCSs in the present simulation is 0.36, which is consistent with that found by Spitler et al. (2007). We note that the Spitler et al. sample includes non-central galaxies.

The mean formation epochs of MPCs and MRCs for all GCs formed in the simulation between $z = 41$ and $z = 0$ are estimated to be 5.7 and 4.3, respectively. These results imply typical ages of MPCs and MRCs at $z = 0$ are 12.7 and 12.3 Gyr, respectively. This is consistent with the current spectroscopic measurements of extragalactic GCs (e.g. Brodie & Strader 2006). The mean values of the number fractions of young GCs with ages less than 8 Gyrs (f_y) is very small ($\leq 4\%$) in the present simulation. Fig. 10 shows that f_y does not depend on B/T . The dependence of f_y on M_B appears to show no/little trend: although f_y appear to peak around $M_B = -19$, this apparent trend is of little statistical significance. owing to the large dispersions. Dispersions in the

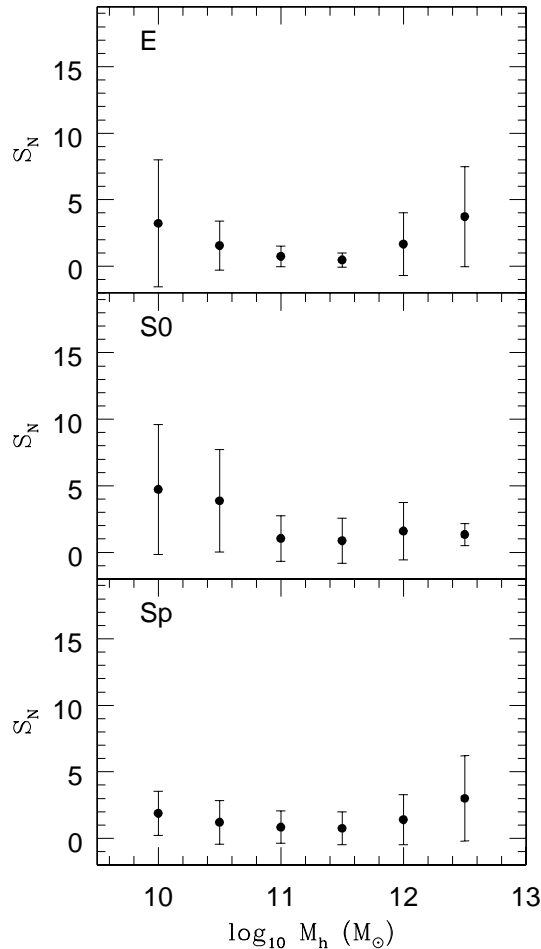


Figure 14. Distributions of the simulated GCSs in the S_N - M_h plane for E (top), S0 (middle), and Sp (bottom). Circles with error bars show the average values of S_N in M_h bins. The 1σ dispersion for each bin is shown by an error bar.

locations of galaxies in the $B/T - f_y$ and the $M_B - f_y$ planes reflect the diversity in the formation epochs of young MRCs, which are mostly via gas-rich major merging.

Next we investigate correlations between mean metallicities of GCs (simply referred to as $[\text{Fe}/\text{H}]$) and M_B of their host galaxies. These correlations are called “metallicity-luminosity relations” for convenience in the present study. The observed metallicity-luminosity relations by P06, after transformation from observed colours, can be described as follows:

$$[\text{Fe}/\text{H}] = a + bM_B \quad (11)$$

The values of the observed coefficients a_o and b_o for MPCs, MRCs, and all GCs are summarized in Table 2. The values of our simulated a_s and b_s using the same relation are listed also in Table 2 for comparison.

Fig. 11 shows that the mean metallicities of *all GCs* correlate well with M_B such that the metallicities are higher in more luminous galaxies. The simulated slope of the $[\text{Fe}/\text{H}] - M_B$ correlation for all GCs is consistent with the observed one by P06 for non-central galaxies. The simulated $[\text{Fe}/\text{H}] - M_B$ correlation for MRCs is also consistent with the observed one which suggests that the present formation model for MRCs is realistic. The $[\text{Fe}/\text{H}] - M_B$ correlation for

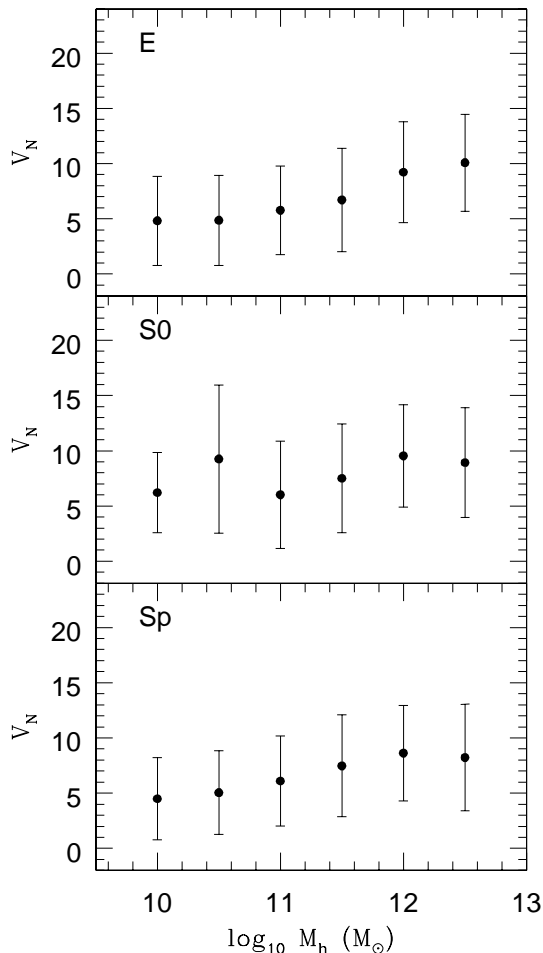


Figure 15. The same as Fig. 14 but for the V_N - M_h plane.

Table 3. Mean S_N and V_N in different Hubble types

	Sp	S0	E
$\langle S_N \rangle$	1.8	2.0	4.0
$\langle V_N \rangle$	8.3	11.4	11.5

MPCs is, however, not so consistent with the observed one: the slope of the correlation is too flat and the mean metallicities of MPCs are systematically higher than the observed ones for a wide range of luminosities. One way to solve this inconsistency is discussed later in §4.3.

3.3 Specific Frequencies S_N and V_N

We investigate specific frequencies (S_N) of GCSs in galaxies with different Hubble types. S_N is defined as follows (Harris & van den Bergh 1981):

$$S_N = N_{\text{gc}} 10^{0.4(M_v + 15)}, \quad (12)$$

where N_{gc} and M_v are the total number of globular clusters in a galaxy and the V -band absolute magnitude of the galaxy, respectively. We also investigate the number of GC per unit halo mass V_N , which, following Spitler et al. (2007), is defined as follows:

$$V_N = N_{\text{gc}} \left(\frac{M_h}{10^{11} M_\odot} \right)^{-1} \quad (13)$$

where M_h is the total mass in a galaxy halo including dark matter. The mean values of S_N and V_N in GCSs of galaxies of different Hubble types are summarized in Table 3. We estimate the 1σ dispersion in S_N and V_N for M_B and M_h bins to investigate the statistical significance in the simulated correlations of S_N and V_N with M_B and M_h . In estimating these dispersions, we use the simulated galaxies with S_N (V_N) less than 20 to avoid unreasonably large dispersions caused by a very small number of galaxies with unusually large S_N (> 50).

Fig. 12 shows that S_N of E/S0s are typically higher than those of spirals (Sp) for a given M_B . Although more luminous Es with $M_B < -20$ have higher S_N than intermediate-luminosity Es with $-19 < M_B < -17$, there is no such a trend in spirals (Sp). Faint galaxies with $M_B > -15$ show high S_N (> 4) which for E/S0 is due to high halo mass-to-light-ratios (M_h/L_B). The mean S_N for Sp, S0, and E populations are 1.8, 2.0, and 4.0, respectively.

Fig. 13 shows that the dependences of V_N on the Hubble types of galaxies are not as strong as those of S_N : only a factor of 2–3 difference in V_N between E/S0 galaxies and spirals for a given luminosity. For a given Hubble type, V_N does not depend strongly on M_B . These results mean that the numbers of GCs per unit halo mass (M_h) does not depend strongly on luminosity or the Hubble type of their host galaxies. The weak dependence of V_N on M_h was already pointed by Bekki et al. (2006, B06), though V_N is estimated only for MPCs in B06.

There is a weak tendency for more luminous Es with $M_B < -20$ mag to have higher V_N , though the dispersion in V_N is large. S0s have V_N values > 8 that are significantly higher than those of spirals for a wide range of M_B , suggesting that the higher V_N in S0s is not due to the truncation of star formation in spirals as V_N does not change when a disk fades via truncation of star formation. These results imply that if the observed V_N are typically higher in S0s than in spirals, then only a minor fraction of spirals can be transformed into S0s via truncation of star formation in spirals.

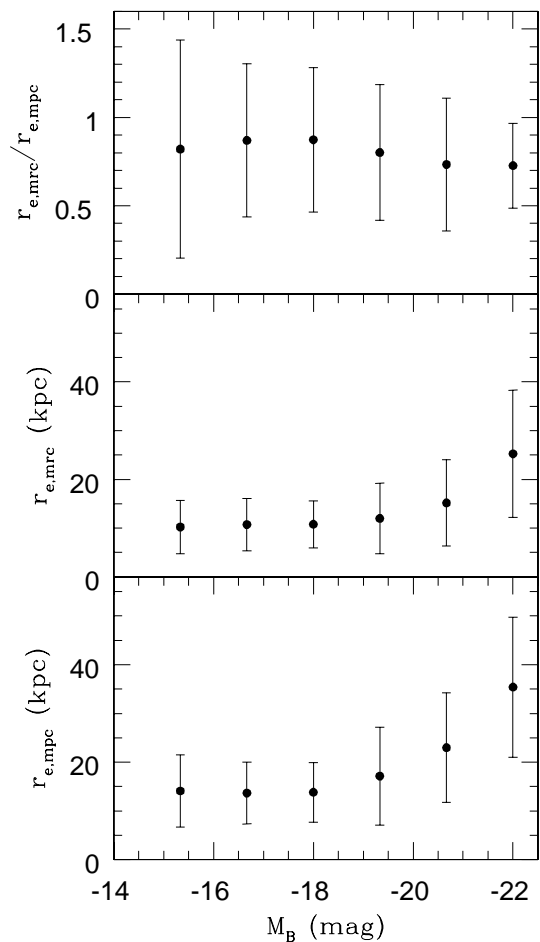
Fig. 14 shows an “U-shape” distribution in the $S_N - M_h$ results for Es, although error bars are quite large (up to ~ 5 for low-mass halos). This U-shape distribution means that S_N is higher in smaller M_h below the threshold halo mass ($M_{h,\text{th}}$) of $\log_{10} M_{h,\text{th}} = 10^{11} M_\odot$ whereas it is higher in larger M_h above $M_{h,\text{th}}$. This simulated distribution for Es appears to be broadly consistent with the latest observation by Peng et al. (2008) for GCSs in the Virgo cluster of galaxies. This U-shape distribution can be also seen in spirals, though it is not so clear in S0s. The $S_N - M_h$ relation for halo masses smaller than $M_{h,\text{th}}$ is due mainly to the fact that M_h/L_B depends strongly on M_h (or on M_B). The $S_N - M_h$ relation for halo masses larger than $M_{h,\text{th}}$ is due mainly to the fact that numbers of GCs per unit halo mass are higher in more massive galaxies.

As shown in Fig 15, the U-shape distributions are less well defined for the $V_N - M_h$ results of galaxies with different Hubble types. However, V_N in galaxies with $M_h > M_{h,\text{th}}$ are significantly higher in Es, which means higher numbers of GCs per unit halo mass in more massive Es. More luminous spirals show higher V_N for $\log M_h < 10^{11.5} M_\odot$. It is not so clear why S0s have V_N values higher than those of Es and Sps at low masses $\log M_h < 10^{10.5} M_\odot$.

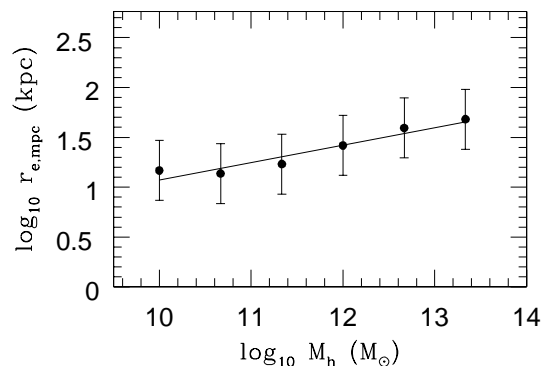
Table 4. Mean properties of the simulated GCSs.

$\langle z_{f,\text{mpc}} \rangle$	$\langle z_{f,\text{mrc}} \rangle$	$\langle f_{\text{bimo}} \rangle$	$\langle f_{\text{mrc}} \rangle$	$\langle f_y \rangle$	$\langle S_N \rangle$	$\langle V_N \rangle$	$\langle s_{\text{eff}} \rangle$	$\langle s_{\text{dis}} \rangle$	$\langle \epsilon \rangle$
5.7	4.3	0.52	0.36	0.04	2.11	11.25	0.84	0.98	0.0013

- a* The mean formation epoch of all MPCs in the simulation.
b The mean formation epoch of all MRCs in the simulation.
c The mean number fraction of galaxies with GCSs showing clear bimodal MDFs.
d The mean number fraction of MRCs in GCSs.
e The mean number fraction of young GCs with ages younger than 8 Gyrs in GCSs.
f The mean S_N (GC number per unit luminosity) in galaxies with GCs.
g The mean V_N (GC number per unit halo mass) in galaxies with GCs.
h The mean ratio of half-number radii of MRCs to those of MPCs in GCSs.
i The mean ratio of velocity dispersions of MRCs to those of MPCs in GCSs.
j The mean net formation efficiency of GCs in galaxies.


Figure 16. Dependences of $r_{e,\text{mrc}}/r_{e,\text{mpc}}$ (top), $r_{e,\text{mrc}}$ (middle), and $r_{e,\text{mpc}}$ (bottom) with M_B . The values averaged for GCSs in M_B bins are shown by filled circles. The 1σ dispersion for each bin is shown by an error bar.

The results in Figs. 14 and 15 thus show that S_N and V_N are fairly high in Es located in the centers of massive halos with $\log M_h \sim 10^{12.5} M_\odot$. These results suggest that giant elliptical galaxies (and cDs) in the centers of massive groups and clusters of galaxies have higher S_N and V_N than those in the field and small groups of galaxies.


Figure 17. Dependence of $r_{e,\text{mpc}}$ (i.e., the half-number radius of a GCS) on M_h (halo mass of the host). The values averaged for GCSs in M_h bins are shown by filled circles. The 1σ dispersion for each bin is shown by an error bar. The χ -square fit to the simulation data is shown by a solid line.

3.4 Dynamical properties

3.4.1 Structures

We next investigate the half-number radii of MPCs ($r_{e,\text{mpc}}$) and MRCs ($r_{e,\text{mrc}}$) for GCs within the virial radii (r_{vir}) of host galaxy dark matter halos: it should be stressed that the results below might well depend weakly on the adopted initial distributions of GCs within their host halos at high z . The spatial distributions of MPCs have valuable information of dark matter halos of their host galaxies (B07). In order to avoid contributions from intracluster and intragroup GCs in groups and clusters of galaxies with $r_{\text{vir}} > 100$ kpc, we estimate $r_{e,\text{mpc}}$ and $r_{e,\text{mrc}}$ within 100 kpc for these groups and clusters. We define s_{eff} to be:

$$s_{\text{eff}} = \frac{r_{e,\text{mrc}}}{r_{e,\text{mpc}}}. \quad (14)$$

We also define the power-law slope (γ) and the coefficient (D_0) of the following relation:

$$r_{e,\text{mpc}} = D_0 M_h^\gamma. \quad (15)$$

Fig. 16 shows that $r_{e,\text{mpc}}$ and $r_{e,\text{mrc}}$ depend on M_B such that both are larger for more luminous galaxies. The mean values of $r_{e,\text{mpc}}$ are larger than 10 kpc for $-22 < M_B < -14$. This is larger than the observed the half-number radius of the Galactic GC system which is about 5 kpc (e.g., van den Bergh 2000). Although no observational studies have so far

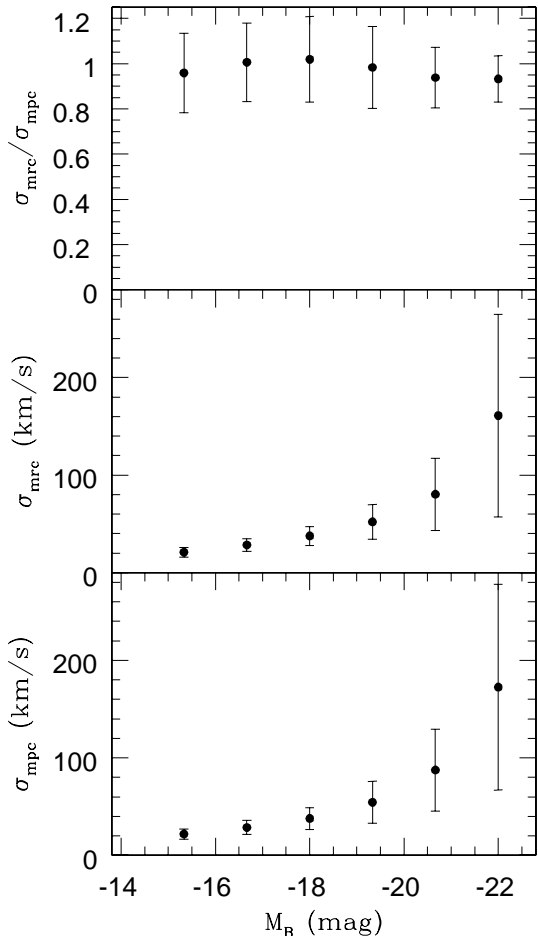


Figure 18. Dependences of $\sigma_{\text{mrc}}/\sigma_{\text{mpc}}$ (top), σ_{mrc} (middle), and σ_{mpc} (bottom) on M_B in the simulation. The values averaged for GCSs at each of the six M_B bins are shown by triangles. The 1σ dispersion for each bin is shown by an error bar.

investigated the correlation of $r_{\text{e,mpc}}$ with M_B , the above results imply that the simulation significantly overestimates $r_{\text{e,mpc}}$: this may be true for MRCs as well. In the present model, all GCs within r_{vir} (virial radius) of the dark matter halo of their host galaxy are used for estimation of $r_{\text{e,mpc}}$. This way of estimating $r_{\text{e,mpc}}$ would contribute significantly to the possible overestimation of $r_{\text{e,mpc}}$ of GCSs in the simulation.

We find s_{eff} is significantly less than 1 for a wide range of luminosities, which means that the distributions of MRCs are more compact than those of MPCs for most GCSs. The mean s_{eff} is 0.84 in the present model, which can not be currently compared with observations owing to the lack of observational studies of s_{eff} in galaxies. The smaller mean value of s_{eff} and the weak dependence of s_{eff} on M_B can be tested against future observational studies. We also suggest that the slopes of $r_{\text{e,mpc}} - M_B$ and $r_{\text{e,mrc}} - M_B$ relations can be used to constrain theoretical models of GC formation based on hierarchical clustering scenarios, because these depend on merging histories of galactic building blocks that form GCs.

Fig. 17 shows $r_{\text{e,mpc}}$ of GCSs correlate with their host halo mass such that $r_{\text{e,mpc}}$ is larger for larger M_h . The χ -square fit to the simulation data is:

$$\log_{10}\left(\frac{r_{\text{e,mpc}}}{\text{kpc}}\right) = -0.69 + 0.18\log_{10}\left(\frac{M_h}{M_\odot}\right) \quad (16)$$

which means $r_{\text{e,mpc}} = 0.20\left(\frac{M_h}{M_\odot}\right)^{0.18}$ kpc (i.e., $\gamma=0.18$). The following equation would be more useful for making an estimation of M_h for a galaxy by measuring $r_{\text{e,mrc}}$ of the GCS:

$$\log_{10}\left(\frac{M_h}{M_\odot}\right) = 4.5 + 5.2\log_{10}\left(\frac{r_{\text{e,mpc}}}{\text{kpc}}\right). \quad (17)$$

Since the present model based on a dissipationless simulation can overestimate $r_{\text{e,mpc}}$, it might be better to use observations in order to determine the zero-point of the above power-law relation. If we use observations of the Galactic GCS (e.g., van den Bergh 2000 and references therein) and the total mass of the Galaxy (Wilkinson & Evans 1999), then the power-law relation is $r_{\text{e,mpc}} = 5.0\left(\frac{M_h}{2 \times 10^{12} M_\odot}\right)^{0.18}$ kpc or $M_h = 2 \times 10^{12} \left(\frac{r_{\text{e,mpc}}}{5 \text{kpc}}\right)^{5.2} M_\odot$. The derived M_h from $r_{\text{e,mpc}} - M_h$ relations can be compared with M_h derived from kinematics of GCSs and halo field stars (e.g., Romanowsky 2006).

3.4.2 Kinematics

A growing number of observational data sets on the kinematical properties of GCSs have been recently accumulated (e.g., Romanowsky 2006). We investigate correlations between velocity dispersions (σ) for MPCs (σ_{mpc}) and MRCs (σ_{mrc}) and M_B of their host galaxies. We first estimate σ_{mpc} and σ_{mrc} of a GCS for each of the three projections (x - y , x - z , and y - z) by using line-of-sight-velocities of all GCs within the virial radius of the halo. We then make an average for the three projections and determine one-dimensional velocity dispersions of σ_{mpc} and σ_{mrc} . We also investigate correlations between M_B and s_{dis} , where s_{dis} is defined as:

$$s_{\text{dis}} = \frac{\sigma_{\text{mrc}}}{\sigma_{\text{mpc}}}. \quad (18)$$

Fig. 18 shows that both σ_{mpc} and σ_{mrc} are higher in more luminous galaxies. The essential reason for this dependence is described as follows. Since the GCSs investigated in the present study are for galaxies located in the centers of dark matter halos (i.e., GCSs in satellite galaxies are not investigated), more luminous galaxies are more likely to be embedded in more massive halos (i.e., larger M_h). GCs follow structures and kinematics of underlying dark matter halos so that the mean velocity dispersions of GCSs are determined mainly by masses of their halos (and by their spatial distributions). Therefore the velocity dispersions of GCSs are higher in more luminous galaxies. The difference in s_{dis} for different M_B is quite small and the mean value of s_{dis} is 0.98. These results imply that velocity dispersions are not so different between MPCs and MRCs in galaxies.

Owing to the collisionless nature of the present simulation, the ratios of maximum rotational velocities to central velocity dispersions (V/σ) in GCSs appear to be low ($V/\sigma < 0.3$) for most galaxies. These results are in a striking contrast with our previous simulations (Bekki et al. 2005) in which some GCSs in the remnants of disk-disk major mergers show large V/σ (> 0.5). Owing to the lack of extensive statistical studies on V/σ of GCSs in galaxies, it is not clear whether the above results are generally consistent with observations or not.

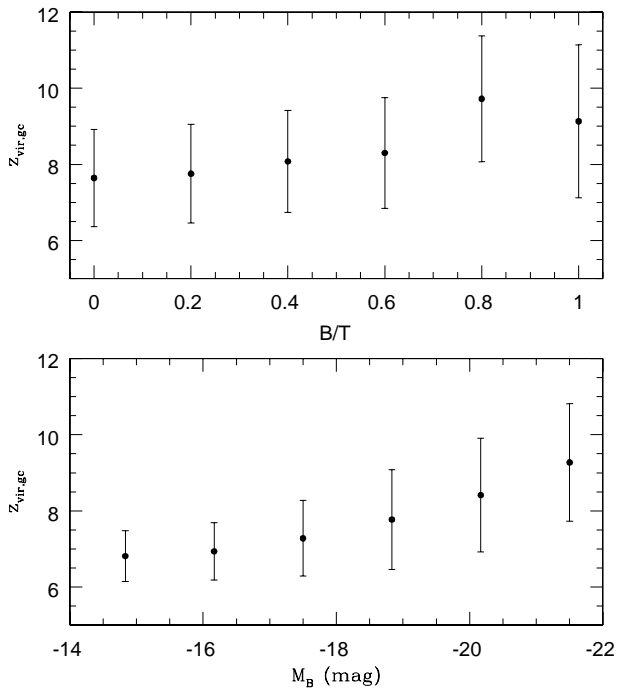


Figure 19. Distributions of the simulated galaxies with GCs in the $z_{\text{vir,gc}} - B/T$ plane (upper) and $z_{\text{vir,gc}} - M_B$ plane (lower) where $z_{\text{vir,gc}}$ is the mean z_{vir} of building blocks hosting GCs in a galaxy. Circles show mean values in B/T and M_B bins. The 1σ dispersion for each bin is shown by an error bar. No galaxies have $z_{\text{vir,gc}} < 6$, because formation of GCs in the present model is truncated for galaxies with $z_{\text{vir}} < 6$.

3.5 Mean properties

Lastly, we briefly summarize the key physical properties of GCs averaged over all GCSs in the simulation in Table 4. The columns are the mean properties of $z_{f,\text{mpc}}$ (column 1), $z_{f,\text{mrc}}$ (2), f_{bimo} (3), f_{mrc} (4), f_y (5), S_N (6), V_N (7), s_{eff} (8), s_{dis} (9), and ϵ (10). In estimating these mean values, we do not include galaxies with no GCs. If we include galaxies with no GCs, the mean values would be significantly changed, in particular, for S_N and V_N .

4 DISCUSSION

4.1 Bimodal colour distributions in GCSs

The origin of the observed bimodal colour distributions of GCSs in elliptical galaxies have long been discussed in the context of different formation scenarios of elliptical galaxies, such as two-phase collapse at high redshift (Forbes et al. 1997), accretion and stripping of low-mass galaxies with GCs (Côte et al. 1998), and gas-rich major mergers (Ashman & Zepf 1992). B02 was the first to investigate the bimodal colour distributions in a quantitative manner based on the results of a semi-analytic model of galaxy formation. B02 showed that the observed bimodality can be reproduced, if MRCs are formed during dissipative merger events at high redshift and that the formation of MPCs are truncated at $z \sim 5$. B02 however did not constrain the truncation mechanism.

Since age differences between MPCs and MRCs are

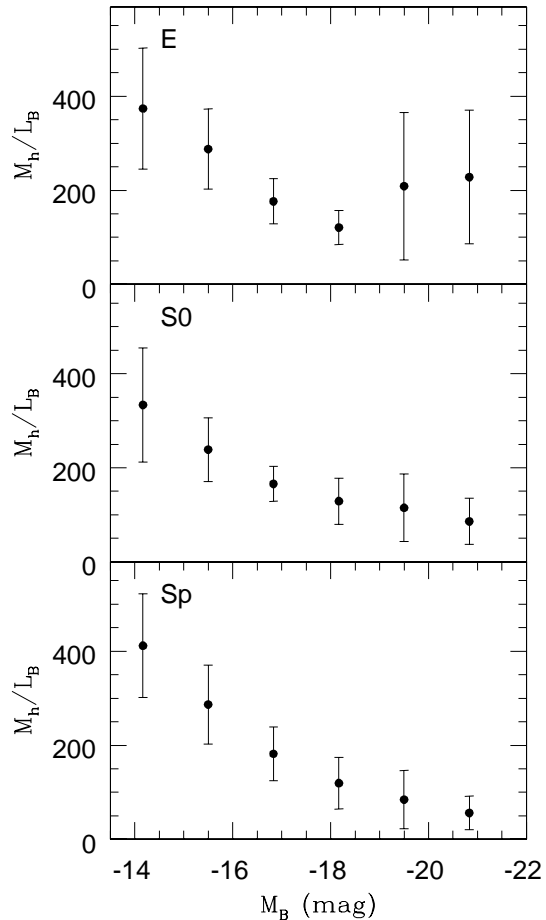


Figure 20. Distributions of the simulated galaxies with GCs in the $M_h/L_B - M_B$ plane, where L_B is the total B -band luminosity of a galaxy, for E (top), S0 (middle), and Sp (bottom). Circles show mean values in M_B bins. The 1σ dispersion for each bin is shown by an error bar.

rather small (< 1 Gyr) in the present simulation, we can discuss the simulated MDFs of GCSs in terms of the colour bimodality of GCSs. In the present model, all GCs (i.e., both MPCs and MRCs) in a galaxy originate from low-mass building blocks at $z > 3$, whether they are isolated or in merging galaxies. Therefore the origin of MRCs in a galaxy is not necessarily associated with the past major merger events of a galaxy. The peak metallicity in the MDF for MPCs (MRCs) in a galaxy reflects the highest GCFR in the galaxy's building blocks that have stellar metallicities lower (higher) than -1 ($[\text{Fe}/\text{H}] \geq -1$). The mean metallicity of MPCs (MRCs) in a galaxy is determined by the mean stellar metallicity of the more metal-poor building blocks with $[\text{Fe}/\text{H}] < -1$ ($[\text{Fe}/\text{H}] \geq -1$). Although MRCs are formed later in more metal-rich building blocks of galaxies, there is only a slight difference in formation redshifts between MPCs and MRCs. The major merger events in which MRCs are formed are typically $z > 3$ whereas the last major merger events which determine the final morphological types of galaxies can happen later at lower redshifts. Therefore the last major merger events responsible for elliptical galaxy formation are not necessarily associated with the formation of MRCs, which is in contrast to the scenario proposed by Ash-

man & Zepf (1992) but consistent with the so-called ‘damp’ merger interpretation of Forbes et al. (2007).

In order to show the key requirements for the formation of bimodal MDFs in GCSs, we have run two comparative models with $\alpha = 0.1$ and $\beta = 0.05$ and $\alpha = 0.02$ and $\beta = 0.25$ (see section 2.3). For these models, the dependences of the GCFR on f_m and f_g are assumed to be very weak. We find that GCSs in these models show much reduced MDF bimodality in comparison with the present standard model with $\alpha = 0.02$ and $\beta = 0.05$ shown in Table 1 (the results of the models are shown in the Appendix B). These results clearly show that a strong enhancement in the GCFR during violent merging (in particular, major merging) and gas-rich phases (i.e., at high redshifts) is important for the formation of the bimodality.

The origin of the metal-poor GC peaks is due mainly to the strong enhancement of the GCFR in gas-rich and high gas-density building blocks at high- z whereas that of the metal-rich ones is due mainly to the strong enhancement of the GCFR in more metal-rich and gas-rich building blocks that experience violent merging at somewhat later epochs. The truncation of GC formation via reionization is necessary for the present model in order to prevent too many GCs from forming in low-mass galaxies. The epoch of reionization, however, appears not to determine the presence of bimodality itself. Although differences in the merging histories of halos between different galaxies can introduce a diversity in GCS properties, such differences appear to have no *direct* link with the resulting bimodal MDFs of the GCSs.

As shown in Fig. 8, not all of galaxies have GCSs with bimodal MDFs. In order to understand why these galaxies have GCSs without bimodality, we have investigated formation histories of GCs in these galaxies (the results for some galaxies are shown in the Appendix B). We find that these galaxies have only either metal-poor or metal-rich peaks in their MDFs owing to single burst events of GC formation. Galaxies with no, or little, enhancement in the GCFR for metal-poor GCs and strong enhancement of the GCFR for metal-rich GCs have no clear bimodality in their MDFs. On the other hand, those with strong enhancement of the GCFR for metal-poor GCs at high z and no enhancement of the GCFR for metal-rich GCs do not show the bimodality either. The efficient formation of MPCs is highly unlikely for galaxies with lower z_{vir} whereas MRCs are highly unlikely to be formed in gas-poor merging at later epochs. The galaxies having GCSs without bimodal MDFs thus have either lower z_{vir} or few events of gas-rich merging and accretion of more metal-rich galactic building blocks.

The present model has shown that a significant fraction ($f_{\text{bimo}} \sim 0.2$) of very late-type spirals with small or no bulges ($B/T < 0.05$) have bimodal MDFs in their GCSs. This is because more metal-rich ($[\text{Fe}/\text{H}] \geq -1$) building blocks of late-type spiral galaxies can form GCs at high z which are later accreted during mergers. Therefore the origin of MRCs (and thus bimodal MDFs) in late-type spiral galaxies are not necessarily associated with the formation of galactic bulges via early major merger events in the present model (see B02 for a brief discussion on this issue). If most bulge-less spirals are found to contain very few MRCs (as appears to be the case for M33; Chandar et al. 2006) then the model proposed here may require significant alteration.

4.2 Specific Frequencies S_N and V_N

Previous observations have revealed that the S_N of GCSs depends on the Hubble type and luminosity of the host galaxy (e.g., Harris 1991; but see also Spitler et al. 2007 for an alternative view). Although the observed trends of S_N with galactic properties (e.g., the bimodality in the $M_V - S_N$ relation) are well reproduced by B06, other key observations of S_N have not been discussed. In the present study, we have shown that (i) S_N of GCSs in luminous galaxies with $M_B < -19$ mag are significantly higher in early-type (E/S0) galaxies than late-type (Sp) ones, (ii) S0s typically have higher S_N than spirals, and (iii) low-luminous galaxies with $M_B > -15$ mag have higher S_N , regardless of their Hubble types. These results are qualitatively consistent with previous observations by Harris (1991), Forbes (2005), and Aragón-Salamanca et al. (2006). So far we have not discussed the physical reasons for the above dependences of S_N on galactic properties.

Fig. 19 shows that the mean values ($z_{\text{vir,gc}}$) of virialization redshifts (z_{vir}) of galactic building blocks that form GCs are significantly higher in early-type galaxies with $B/T > 0.8$ than in late-type ones. This means that GCFRs in building blocks of early-type galaxies are higher owing to their higher mass-densities with higher z_{vir} . Because GCFRs depends strongly on z_{vir} through the term of F_z (see equation 6) the higher $z_{\text{vir,gc}}$ in early-type galaxies is one reason for the observed higher S_N of their GCSs. Furthermore Fig. 19 shows that $z_{\text{vir,gc}}$ is higher in more luminous galaxies, which can explain why more luminous early-type galaxies with $M_B < -19$ mag are more likely to have higher S_N in comparison with less luminous ones with $-19.0 < M_B < -17$ mag seen in Fig. 12.

Fig. 19 shows that low-luminosity galaxies do not have higher $z_{\text{vir,gc}}$, which implies that higher S_N in low-luminosity galaxies seen in Fig. 9 can not be understood in terms of $z_{\text{vir,gc}}$. B06 suggested that the origin of the observed higher S_N in low-luminosity galaxies is due to higher mass-to-light-ratios ($M/L \approx M_h/L_B$) of these galaxies. Fig. 20 shows that M_h/L_B steeply depends on luminosity in the sense that M_h/L_B is higher in less luminous galaxies. Given that GC numbers per unit halo mass (V_N) in galaxies only weakly depend on the halo masses of the galaxy (B06; see also Fig.13 in the present paper), the above result implies that the higher S_N in low-luminosity galaxies are due mainly to their higher M_h/L_B ratios owing to the relation $S_N = V_N (\frac{M_h}{L_B})$.

4.3 Metallicity-luminosity relations

Although B02 predicted that the mean colours of both MPCs and MRCs only weakly correlate with the total luminosities of their host galaxies, these predictions are inconsistent with latest observations by Strader et al. (2004) and P06. The present model has successfully reproduced reasonably well, the observed $[\text{Fe}/\text{H}] - M_B$ relations for MRCs and all GCs. The derived slope in the $[\text{Fe}/\text{H}] - M_B$ relation for MPCs in the present model is, however, not consistent with the observed one. The differences between B02 and the present study are caused by the differences in the adopted models of GC formation between these two studies. Thus more sophisticated models of GC formation in galaxies at high z need to be developed so that all three $[\text{Fe}/\text{H}] - M_B$

Table 5. Qualitative assessment of model successes and failures.

Items	Consistency ^a	Comments
Ages	○	Data indicate very old ages for both MRCs and MPCs.
Bimodal MDFs	○	Requires predicted MDFs in observed colours.
$f_{\text{bimo}} - M_{\text{B}}$	○	Broadly consistent but data very limited.
$f_{\text{mrc}} - M_{\text{B}}$	○	Consistent with data for luminous galaxies.
f_{y}	○	Broadly consistent but data very limited.
$M_{\text{B}} - [\text{Fe}/\text{H}]$	○	Less consistent for MPCs.
$S_{\text{N}} - B/T$	○	Consistent in terms of higher S_{N} in Es.
$S_{\text{N}} - M_{\text{B}}$	△	U-shape of data not clearly seen.
$V_{\text{N}} - M_{\text{h}}$	△	Data show a flatter slope.
$r_{\text{e,mpc}}$	△	Data for the Galaxy is much smaller.

^a ○ (×) means that simulations are broadly consistent (inconsistent) with observations. △ means that simulations are only partly consistent with observations.

relations (MPCs, MRCs, and all GCs) can successfully reproduce the observations.

B07 showed that if $z_{\text{trun}} \approx 10$, the observed $[\text{Fe}/\text{H}] - M_{\text{B}}$ relation for MPCs is better reproduced. However the simulated ϵ (i.e., the formation efficiency of GCs) in the model with $z_{\text{trun}} = 10$ in the present study is too small (0.00077) to be consistent with the observed one by McLaughlin (1999). The present model seems to have difficulties in explaining self-consistently both the observed $[\text{Fe}/\text{H}] - M_{\text{B}}$ relation for MPCs and ϵ . One possible way to solve this problem would be to investigate models with higher z_{trun} ($=6 - 10$) in which C_{eff} depends more strongly on z than in the present model so enough GCs can be formed at $z = 6 - 10$. It is, however, unclear whether the models with higher z_{trun} and C_{eff} can reproduce other key observations such as the $S_{\text{N}} - M_{\text{B}}$ relation.

4.4 Success and failures of the present model

Although we have so far presented variously different physical properties of GCSs in galaxies, only some of them can be directly compared with observations: for example, the simulated $f_{\text{mrc}} - M_{\text{B}}$ relation can be compared with observations by P06 whereas the simulated $s_{\text{dis}} - M_{\text{B}}$ one can not owing to the lack of observational data. It is, however, important to check whether the simulated properties are consistent with the corresponding observations. In Table 5 we summarise what we regard as the relative successes and failures of the current model in a qualitative sense. For any given physical property there are subtle, and sometimes large, differences between the observational data and the corresponding property predicted by the model. The references of these observational properties are already given in the Introduction section §1 (e.g., Brodie & Strader 2006) and some of the observational data are presented within figures of this paper. Less consistent results (e.g., the $M_{\text{B}} - [\text{Fe}/\text{H}]$ relation for MPCs) imply that a more sophisticated model for GC formation would be required for more successful modeling.

5 CONCLUSIONS

We have investigated the structural, kinematical, and chemical properties of globular cluster systems (GCSs) in galaxies

in a self-consistent manner based on high-resolution cosmological N-body simulations combined with a semi-analytic model of galaxy and globular cluster (GC) formation. We have adopted a number of assumptions on formation efficiencies of GCs which depend on the physical properties of their host galaxies (e.g., gas mass fraction). We investigated correlations between physical properties of GCSs and those of their host galaxies for $\sim 10^5$ simulated central halo galaxies for MPCs with $[\text{Fe}/\text{H}] < -1$ and MRCs with $[\text{Fe}/\text{H}] \geq -1$.

We find: (1) The majority ($\sim 90\%$) of GCs currently in halos of galaxies are formed in low-mass galaxies at $z > 3$ with mean formation redshifts of MPCs and MRCs being 5.7 and 4.3, respectively. This corresponds to 12.7 and 12.3 Gyrs in lookback time. The majority of MPCs are formed in low-mass galaxies that are virialized well before reionization ($z > 6$) and thus have higher mass densities. MRCs are formed slightly later not only within high z major mergers between high-density galaxies but also within gas-rich isolated ones.

(2) About 50 % of galaxies with GCs show clear bimodalities in their MDFs, though less luminous galaxies with M_{B} fainter than -17 are much less likely to show the bimodalities owing to no or few MRCs. The age differences between MPCs and MRCs are quite small (< 1 Gyr) in most galaxies. The origin of the simulated bimodality in MDFs is due to strong dependences of GCFE on f_{g} and f_{m} (i.e., higher GCFE in more gas-rich high- z galaxies and in mergers with larger mass ratios of the merging two galaxies).

(3) The number fractions of MRCs (f_{mrc}) range from 0 to almost 1 with an average of 0.4. The f_{mrc} in galaxies does not depend on their Hubble type (i.e., bulge-to-disk-ratios), which implies that the formation of MRCs is not necessarily associated with bulge formation. The f_{mrc} are likely to be smaller for less luminous galaxies.

(4) The S_{N} of GCSs are typically higher in ellipticals than in spirals, and in low-luminosity galaxies with $M_{\text{B}} > -15$ regardless of their Hubble types. The mean S_{N} for Sp, S0, and E populations are 1.8, 2.0, and 4.0, respectively.

(5) The number of GCs per halo mass (V_{N}) does not depend as strongly on the luminosity or the Hubble type of the host galaxy as S_{N} does, which suggests that the GC number per unit mass is similar between different galaxies. V_{N} is, however, likely to be higher in luminous ellipticals with $M_{\text{B}} < -20$.

(6) Although there are no significant differences in V_{N} between spirals and S0s for luminous galaxies ($M_{\text{B}} < -20$),

S0s are more likely to have higher V_N than spirals for less luminous galaxies with $M_B > -18$. These results suggest that only luminous S0s with moderately high S_N can be transformed spirals via truncation of star formation and the resultant disk fading, because V_N does not change during disk fading.

(7) The mean metallicities of GCs ($[Fe/H]$) for MPCs and MRCs depend on M_B of their host galaxies such that they are higher in more luminous galaxies, though the dependence for MPCs is weak. Although the observed correlation of $M_B - [Fe/H]$ for MRCs can be well reproduced by the present model, that for MPCs is not consistent with the simulated one. The observed correlation between the mean metallicities of all GCs and M_B can be well reproduced by the present model.

(8) Spatial distributions of MRCs are more compact than those of MPCs with $r_{e,mrc} \sim 0.84r_{e,mpc}$. The $r_{e,mpc}$ depends strongly on halo mass M_h such that $r_{e,mpc} \propto M_h^{0.18}$ (or $M_h \propto r_e^{5.2}$) which implies that $r_{e,mpc}$ can be used for estimating the total masses of dark matter halos.

(9) There is no significant difference in velocity dispersion between MPCs and MRCs. Velocity dispersions are larger in more luminous galaxies both for MPCs and MRCs regardless of their Hubble types.

(10) The physical properties of GCSs such as MDFs, f_{mrc} , S_N , and V_N are quite diverse between different galaxies, depending on the virialization redshifts of their building blocks and subsequent merging, star formation, and chemical evolution histories of the building blocks.

ACKNOWLEDGMENTS

We are grateful to the anonymous referee for valuable comments, which contribute to improve the present paper. K.B. and D.A.F. acknowledge the financial support of the Australian Research Council throughout the course of this work. H.Y. acknowledges the support of the research fellowships of the Japan Society for the Promotion of Science for Young Scientists (17-10511). MN was supported by the Grant-in-Aid for the Scientific Research Fund (18749007) of the Ministry of Education, Culture, Sports, Science and Technology of Japan and by a Nagasaki University president's Fund grant. We are grateful to Lee Spitler for providing observational data and discussing the present results with us. The numerical simulations reported here were carried out on Fujitsu-made vector parallel processors VPP5000 kindly made available by the Center for Computational Astrophysics (CfCA) at National Astronomical Observatory of Japan (NAOJ) for our research project why36b and uhy09a.

REFERENCES

Aragn-Salamanca, A., Bedregal, A. G., Merrifield, M. R., 2006, *A&A*, 458, 101
 Ashman, K. M., Zepf, S. E., 1992, *ApJ*, 384, 50
 Ashman, K. M., Zepf, S. E., 1998, in *Globular cluster systems*, Cambridge, U. K. ; New York : Cambridge University Press,
 Bassino, L. P., Faifer, F. R., Forte, J. C., Dirsch, B., Richtler, T., Geisler, D., Schubert, Y., 2006, *A&A*, 451, 789
 Beasley, M. A., Baugh, C. M., Forbes, D. A., Sharples, R. M., Frenk, C. S. 2002, *MNRAS*, 333, 383

Bekki, K., Forbes, D. A., Beasley, M. A., & Couch, W. J. 2002, *MNRAS*, 344, 1334 (BFBC02)
 Bekki, K., Beasley, M. A., Brodie, J. P., & Forbes, D. A. 2005, *MNRAS*, 363, 1211
 Bekki, K., Forbes, D. A., 2006, *A&A*, 445, 485
 Bekki, K., Yahagi, H., Forbes, D. A., 2006, *ApJL*, 645, 29 (B06)
 Bekki, K., & Yahagi, H., 2006, *MNRAS*, 372, 1019
 Bekki, K., Yahagi, H., Forbes, D. A., 2007, *MNRAS*, 377, 215 (B07a)
 Bergond, G., Zepf, S. E., Romanowsky, A. J., Sharples, R. M., Rhode., 2006, *A&A*, 448, 155
 Bertschinger, E., 1995, *astro-ph/9506070*
 Bertschinger, E., 2001, *ApJS*, 137, 1
 Bridges, T., et al., 2006, *MNRAS*, 373, 157
 Brodie, J. P., Huchra, J. P., 1991, *ApJ*, 379, 157
 Brodie, J. P., Strader, J., 2006, *ARA&A*, 44, 193
 Chandar, R.,; Puzia, T. H., Sarajedini, A., Goudfrooij, P., 2006, *ApJL*, 646, 107
 Cte, P., Marzke, R. O., West, M. J. 1998, *ApJ*, 501, 554
 Cte, P. et al. 2001, *ApJ*, 559, 828
 Davis, M., Efstathiou, G., Frenk, C. S., & White, S. D. M. 1985, *ApJ*, 292, 371
 Fan, X. et al. 2003, *AJ*, 125, 1649
 Forbes, D. A., Brodie, J. P., & Grillmair, C. J., 1997, *AJ*, 113, 1652
 Forbes, D. A., Forte, J. C., 2001, *MNRAS*, 322, 257
 Forbes, D. A., 2005, *ApJL*, 635, 137
 Forbes, D. Proctor, R., Strader, J., Brodie, J. 2007, *ApJ*, 659, 188
 Freeman, K. C. 1993, in *The globular clusters-galaxy connection*, edited by Graeme H. Smith, and Jean P. Brodie, ASP conf. ser. 48, p608
 Harris, W. E., & van den Bergh, S., 1981, *AJ*, 86, 1627
 Harris, W. E. 1986, *AJ*, 91, 822
 Harris, W. E., 1991, *ARA&A*, 29, 543
 Hwang, H. S., et al. 2007, to appear in *ApJ* (*astro-ph/07094309*)
 Jones, J. B., et al., 2006, *AJ*, 131, 312
 Jordn, A. et al, 2006, *ApJL*, 651, 25
 Kissler-Patig, M., Gebhardt, K., 1998, *AJ*, 116, 2237
 Kravtsov, A. V., Gnedin, O. Y., 2005, *ApJ*, 623, 650
 Lada, C. J., & Lada, E. A., 2003, *ARR&A*, 41, 57
 Larsen, S. S.; Richtler, T., 2000, *A&A*, 354, 836 (LR00)
 McLaughlin, D. E., 1999, *AJ*, 117, 2398
 Mo, H. J., Mao, S., White, S. D. M., 1998, *MNRAS*, 295, 319 (Nagashima, M., Yahagi, H., Enoki, M., Yoshii, Y., Gouda, N., 2005, *ApJ*, 634, 26
 Peng, E. W., Ford, H. C., Freeman, K. C., 2004, *ApJ*, 602, 705
 Peng, E., et al. 2006, *ApJ*, 639, 95
 Peng, E., et al. 2008, in preprint
 Pierce, M. et al, 2006, *MNRAS*, 366, 1253
 Rode, K. L., Zepf, S. E., & Santos, M. R. 2005, *ApJL*, 630, 21
 Rhode, K. L., Zepf, S. E., 2004, *AJ*, 127, 302
 Richtler, T. et al. 2004, *AJ*, 127, 2094
 Romanowsky, A. J., 2006, in *the Globular Clusters to Guides to Galaxies*.
 Santos, M. R. 2003, in *Extragalactic Globular Cluster Systems*, Proceedings of the ESO Workshop, p. 348
 Searle, L. & Zinn, R., 1978, *ApJ*, 225, 357 (SZ)
 Simien, F.; de Vaucouleurs, G., 1986, *ApJ*, 302, 564
 Spitler, L. R., Larsen, S. S., Strader, J., Brodie, J. P., Forbes, D. A., Beasley, M. A., 2006, accepted in *AJ* (*astro-ph/0606337*)
 Spitler, L. R. et al., 2007, in preparation.
 Strader, J., Brodie, J. P., Forbes, D. A., 2004, *AJ*, 127, 3431
 Strader, J., Brodie, J. P., Spitler, L., Beasley, M. A., 2006, submitted to *AJ* (*astro-ph/0508001*).
 Susa, H., Umemura, M. 2004, *ApJ*, 600, 1
 van den Bergh, S. 1986, *AJ*, 91, 271
 van den Bergh, S. 2000, *The Galaxies of the Local Group*, Cambridge: Cambridge Univ. Press.

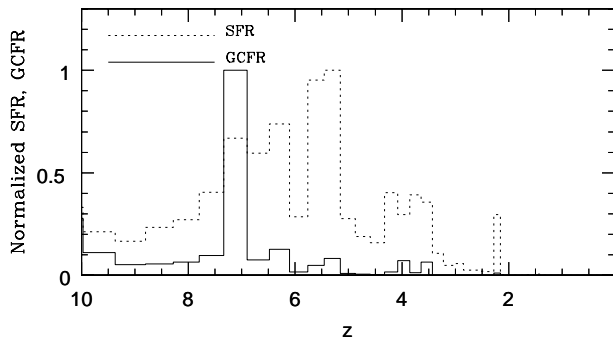


Figure A1. SFR (dotted) and GCFR (solid) as a function of z in an early-type galaxy (G1) located in the central region of a massive cluster of galaxies with $M_h = 6.3 \times 10^{14} M_\odot$. G1 has a $B/T = 1.0$, $M_B = -20.7$ mag, and $M_V = -21.5$ mag. For comparison, the SFR and GCFR normalized by their maximum values are shown.

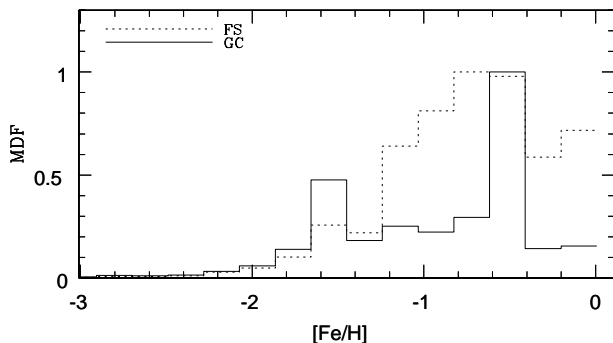


Figure A2. Solid and dotted lines represent the MDF of GCs in the galaxy G1 and that of all field stars (FS) that were formed in galaxies previously hosting the GCs of G1. Note that only the GCS shows a clear bimodal MDF.

West, M. J., Côte, P., Marzke, R. O., Jordán, A., 2004, *Nat*, 427, 31

Wilkinson, M. I., Evans, N. W. 1999, *MNRAS*, 310, 645

Woodley, K. A., Harris, W. E., Beasley, M. A., Peng, E. W., Bridges, T. J., Forbes, D. A., Harris, G. L. H., 2007, *AJ*, 134, 494

Yahagi, H. 2005, *PASJ*, 57, 779

Yahagi, H., & Yoshii, Y. 2001, *ApJ*, 558, 463

Yahagi, H., Nagashima, M., & Yoshii, Y., 2004, *ApJ*, 605, 709

Yahagi, H., Bekki, K., 2005, *MNRAS*, 364L, 86

Zinnecker, H., Keable, C. J., Dunlop, J. S., Cannon, R. D., Griffiths, W. K., 1988, in Grindlay, J. E., Davis Philip A. G., eds, *Globular cluster systems in galaxies*, Dordrecht, Kluwer, p603

APPENDIX A: INDIVIDUAL CASES

Here we briefly discuss some results of GCSs in individual model galaxies (G1 and G2). Fig. A1 shows an elliptical galaxy (G1) at the center of a massive cluster of galaxies with $M_h = 6.4 \times 10^{14} M_\odot$ which has two strong peaks in the GCFR at high redshifts, $z \sim 7$ and ~ 10 . On the other hand, SFRs of building blocks of G1 (including G1) show multiple peaks at $2 < z < 6$, which means that formation of field stars can continue to be quite active till relatively recently. For G1, both the vast majority of field stars and GCs are formed till $z = 2$. Fig. A2 shows that although the MDF of

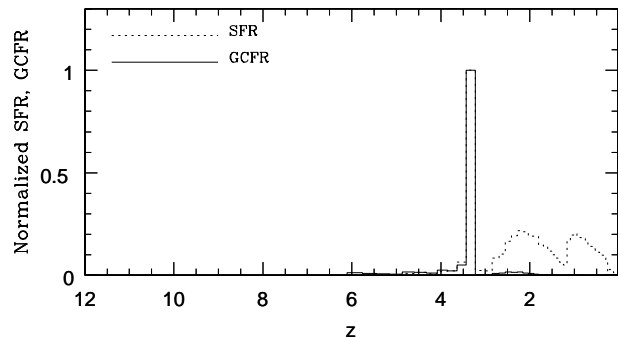


Figure A3. The same as Fig. A1 but for a spiral galaxy G2 with $M_h = 4.1 \times 10^{11} M_\odot$. G2 has a $B/T = 0.13$, $M_B = -18.9$ mag, and $M_V = -19.6$ mag.

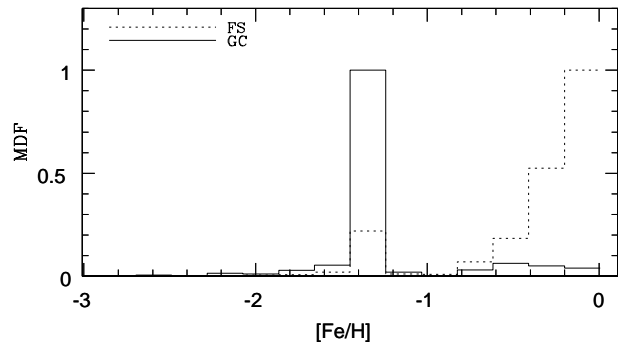


Figure A4. The same as A2 but for a spiral galaxy G2.

GCs shows clearly a bimodality, that of field stars does not. Given that some fraction of *these field stars located in the outer part of G1* can finally become halo field stars in G1 in the present model, the above result suggests that stellar halos of ellipticals can have unimodal MDFs as opposed to bimodal ones seen in their GCSs.

Fig. A3 shows that in a simulated late-type spiral (G2), the vast majority of GCs are formed before $z = 3$ whereas field stars can continue to form till $z = 0$, which is in significant contrast with the results for the cluster ellipticals shown in Fig. A1. It should be stressed here that although building blocks of G2 are virialized before $z = 6$, intensive GC formation happens around ~ 3 . This means that GC formation in G2 is triggered by merging of the building blocks (with $z_{\text{vir}} > 6$) at relatively later redshifts. As shown in Fig. A4, G2 also shows a lower peak metallicity for MRCs ($[\text{Fe}/\text{H}] \sim -0.6$) and a smaller number of MRCs. The peak metallicity for metal-poor field stars is almost coincident with that for MPCs, which suggests that the MDFs are not so different between MPCs and halo field stars in G2. It should be stressed here that some galaxies with M_B , M_h , and Hubble types similar to G2 have shapes of MDFs in GCSs significantly different from that of G2. The variety in merging histories between different galaxies can cause these differences in MDFs.

Fig. A5 shows that the MDFs in spirals embedded in dark matter halos with different halo masses have variously different MDFs: spirals labeled as (a), (c), and (j) show remarkably strong peaks for MPCs owing to a larger number of MPCs whereas those labeled as (b), (e), (h), and (i) show clearly multiple (triple) peaks in MDFs. Spirals labeled as

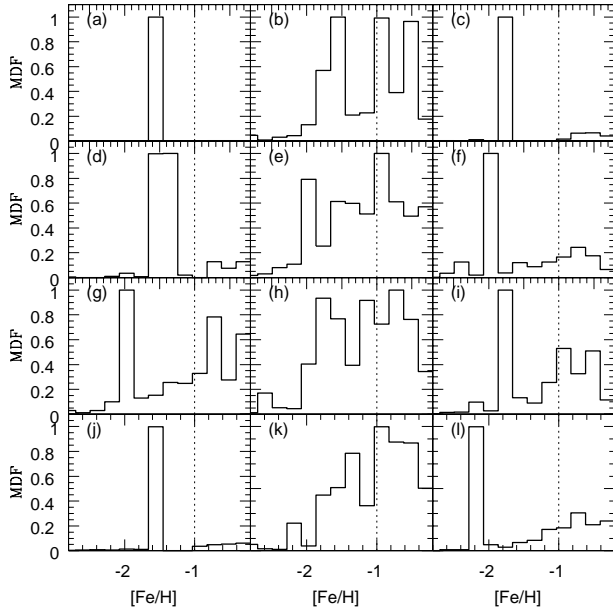


Figure A5. A collection of MDFs of 16 GCSs in spiral galaxies with $B/D < 0.68$ and with different M_h . The 16 spiral galaxies are selected from those embedded in dark matter halos with $11.5 \leq \log_{10}(M_h/M_\odot) \leq 12.0$. Here GCSs are selected such that just one GCS can be allocated in each of 16 equally spaced mass bins in $\log_{10}M_h$ over the above mass range. GCSs in lower M_h are given earlier characters in alphabetical orders: the GCSs in the lowest and highest M_h are labeled as (a) and (l), respectively. The threshold metallicities between MPCs and MRCs (i.e., $[\text{Fe}/\text{H}] = -1$) are shown by dotted lines for comparison.

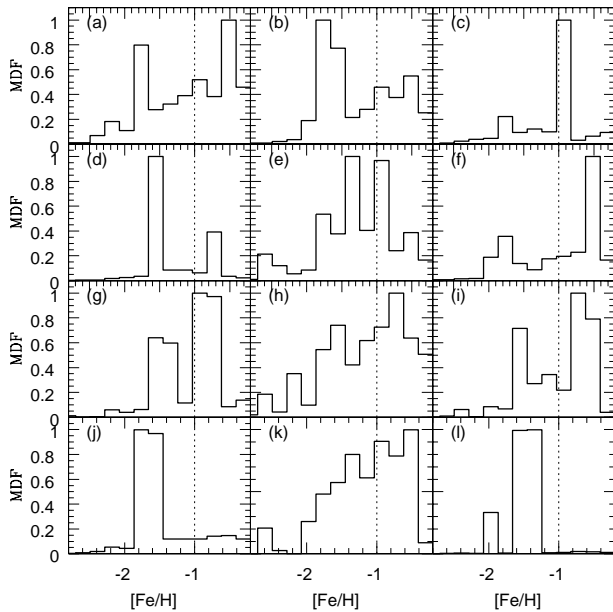


Figure A6. The same as Fig. A5 but for 16 GCSs in early-type (E and S0) galaxies with $B/D \geq 0.68$ and with different M_h . The 16 early-type galaxies are selected from those embedded in dark matter halos with $11.5 \leq \log_{10}(M_h/M_\odot) \leq 13.0$.

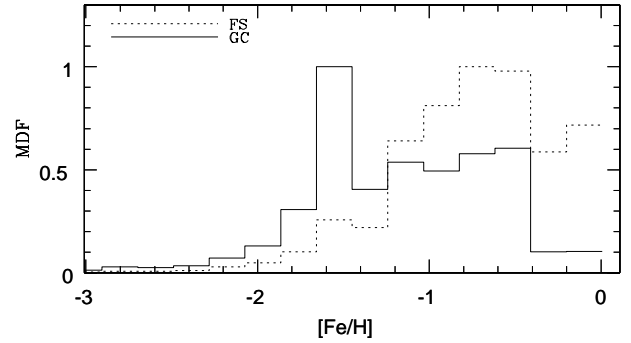


Figure B1. The same as Fig. A2 but for the model with $\alpha = 0.1$ and $\beta = 0.05$.

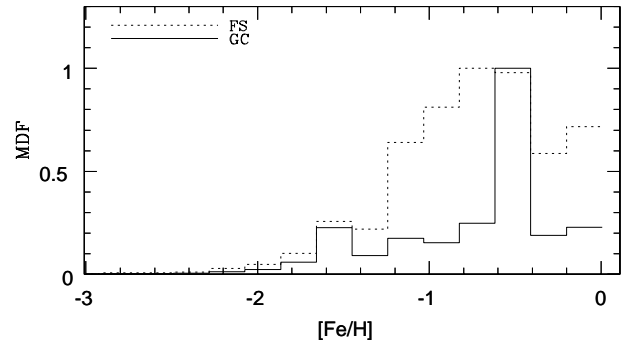


Figure B2. The same as Fig. A2 but for the model with $\alpha = 0.02$ and $\beta = 0.25$.

(f) and (l) can be considered to be showing clearly bimodal MDFs in their GCSs. The relative contributions of MRCs to MDFs are clearly different between different GCSs in these 16 spirals. Fig. A6 shows that MDFs in ellipticals embedded in dark matter halos with different halo masses have variously different MDFs: a larger number of GCSs appear to have bimodal MDFs in ellipticals than in spirals. These diversities in the shapes of MDFs in galaxies with different luminosities and Hubble types reflect the diversities in merging and star formation histories between the galaxies.

APPENDIX B: COMPARATIVE MODELS

We ran models with different α and β in order to more clearly understand the origin of the bimodal MDFs seen in

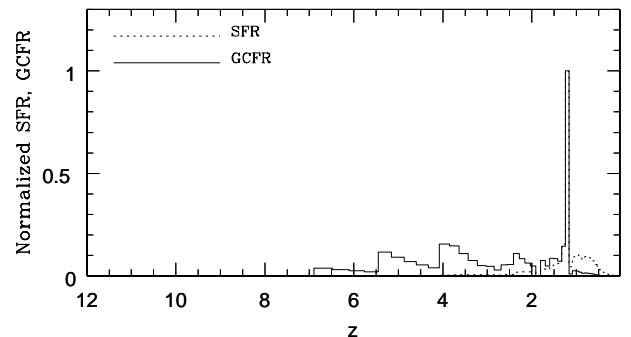


Figure B3. The same as Fig. A1 but for galaxy G3.

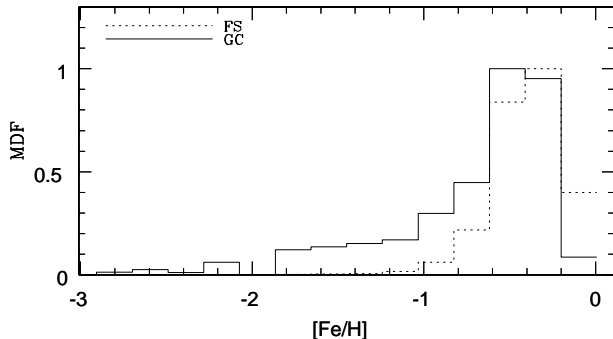


Figure B4. The same as Fig. A2 but for galaxy G3.

the present simulation. Fig. B1 shows the MDF of the galaxy G1 (shown in Figs. A1 and A2) for the model with $\alpha = 0.1$ (i.e., five times larger than that used in the model described in the main text) and $\beta = 0.05$. For this model with very weak dependence of GCFR on f_m owing to a larger value of α , strong enhancement in GCFR during major merging can not happen. The MDF, which can be compared with that in Fig. A1, does not clearly show the metal-rich peak. This means that strong enhancement in the GCFR during violent merging is important for the appearance of bimodality.

Fig. B2 shows the MDF of G1 for the model with $\alpha = 0.02$ and $\beta = 0.25$ (i.e., five times larger than that used in the model described in the main text). For this model with very weak dependence of GCFR on f_g , strong enhancement in GCFR during gas-rich phases (thus mostly at high-redshifts) can not happen. Although the metal-poor peak can be barely seen, the bimodal MDF in this model becomes much less significant than that in the model shown in Fig. A1. This result suggests that strong enhancement of the GCFR in gas-rich phases of galaxies (thus at high-redshifts) can be also important for the formation of the bimodality. Since we assume that galaxies with higher z_{vir} have higher surface mass densities, stronger enhancement of GCFR in more gas-rich galaxies at higher z means high GCFR in galaxies with higher surface densities of gas. These results thus suggest that the origin of the bimodality can result from stronger enhancement of the GCFR in more violent merging and more gas-rich (and higher surface gas density) galactic building blocks.

As shown in Fig. 8 and A6, not all of the simulated GCSs have bimodal MDFs. It is therefore important to clarify the reasons why these GCSs do not have bimodal MDFs. By investigating both MDFs and star formation histories (SFRs) in galaxies having GCSs without bimodality, we find that most of GCSs without bimodality either show only metal-poor peaks or show only metal-rich ones owing to very strong enhancement of the GCFR during single burst epochs of GC formation. Fig. B3 and B4 show the SFH and the MDF, respectively, for the galaxy G3 with $B/T = 0.7$ and $M_h = 2 \times 10^{11} M_\odot$. Owing to the very strong burst of GC formation during late major merging around $z = 1$ for this galaxy G3, too many metal-rich GCs can be formed. This galaxy does not experience strong enhancement of the GCFR before $z = 6$ so that the metal-poor peak in the MDF is not clear. As a result of these, G3 does not show the bimodality in the GCS. G3 is the representative case for galaxies which do not show the bimodality in their GCSs

owing to the too many metal-rich GCs. Other galaxies having GCSs without the bimodality (which are mostly less-luminous systems) do not have metal-rich peaks owing to the lack of strong enhancement of GCFR later in their evolution. The galaxy labeled as (j) with no strong metal-rich peak in Fig. A6 is a good example of such galaxies.